



1 **Uncertainties in eddy covariance air-sea CO₂ flux measurements and**
2 **implications for gas transfer velocity parameterisations**

3
4 **Yuanxu Dong^{1,2}, Mingxi Yang², Dorothee C. E. Bakker¹, Vassilis Kitidis² and Thomas G.**
5 **Bell²**

6 ¹Centre for Ocean and Atmospheric Sciences, School of Environmental Sciences, University
7 of East Anglia, Norwich, UK

8 ²Plymouth Marine Laboratory, Prospect Place, Plymouth, UK

9
10 *Correspondence to:* Yuanxu Dong (Yuanxu.Dong@uea.ac.uk)

11 **Abstract.** Air-sea carbon dioxide (CO₂) flux is often indirectly estimated by the bulk method
12 using the air-sea difference in CO₂ fugacity ($\Delta f\text{CO}_2$) and a parameterisation of the gas transfer
13 velocity (K). Direct flux measurements by eddy covariance (EC) provide an independent
14 reference for bulk flux estimates and are often used to study processes that drive K . However,
15 inherent uncertainties in EC air-sea CO₂ flux measurements from ships have not been well
16 quantified and may confound analyses of K . This paper evaluates the uncertainties in EC CO₂
17 fluxes from four cruises. Fluxes were measured with two state-of-the-art closed-path CO₂
18 analysers on two ships. The mean bias in the EC CO₂ flux is low but the random error is
19 relatively large over short time scales. The uncertainty (1 standard deviation) in hourly
20 averaged EC air-sea CO₂ fluxes (cruise-mean) ranges from 1.4 to 3.2 mmol m⁻² day⁻¹. This
21 corresponds to a relative uncertainty of ~20% during two Arctic cruises that observed large
22 CO₂ flux magnitude. The relative uncertainty was greater (~50%) when the CO₂ flux magnitude
23 was small during two Atlantic cruises. Random uncertainty in the EC CO₂ flux is mostly caused
24 by sampling error. Instrument noise is relatively unimportant. Random uncertainty in EC CO₂
25 fluxes can be reduced by averaging for longer. However, averaging for too long will result in
26 the inclusion of more natural variability. Auto-covariance analysis of CO₂ fluxes suggests that
27 the optimal timescale for averaging EC CO₂ flux measurements ranges from 1–3 hours, which
28 increases the mean signal-to-noise ratio of the four cruises to higher than 3. Applying an
29 appropriate averaging timescale and suitable $\Delta f\text{CO}_2$ threshold (20 μatm) to EC flux data
30 enables an optimal analysis of K .

31



32 1 Introduction

33 Since the Industrial Revolution, atmospheric CO₂ levels have risen steeply due to human
34 activities (Broecker and Peng, 1993). The ocean plays a key role in the global carbon cycle,
35 having taken up roughly one quarter of anthropogenic CO₂ emissions over the last decade
36 (Friedlingstein et al., 2020). Accurate estimates of air-sea CO₂ flux are vital to forecast climate
37 change and to quantify the effects of ocean CO₂ uptake on the marine biosphere.

38 Air-sea CO₂ flux (F , e.g. in mmol m⁻² day⁻¹) is typically estimated indirectly by the bulk
39 equation:

$$40 \quad F = K_{660}(Sc/660)^{-0.5} \alpha(fCO_{2w} - fCO_{2a}) \quad (1)$$

41 Where K_{660} (in cm h⁻¹) is the gas transfer velocity, usually parameterised as a function of wind
42 speed (e.g. Nightingale et al., 2000), Sc (dimensionless) is the Schmidt number (Wanninkhof,
43 2014) and α (mol L⁻¹ atm⁻¹) is the solubility (Weiss, 1974). fCO_{2w} and fCO_{2a} are the CO₂
44 fugacity (in μ atm) at the sea surface and in the overlying atmosphere, respectively, with
45 $fCO_{2w} - fCO_{2a}$ the air-sea CO₂ fugacity difference (ΔfCO_2). Uncertainties in the K_{660}
46 parameterisation and limited coverage of fCO_{2w} measurements result in considerable
47 uncertainties in global bulk flux estimates (Takahashi et al., 2009; Woolf et al., 2019).

48 Eddy covariance (EC) is the most direct method for measuring the air-sea CO₂ flux F :

$$49 \quad F = \overline{\rho w' c'} \quad (2)$$

50 where ρ is the mean mole density of dry air (e.g. in mole m⁻³). The dry CO₂ mixing ratio c (in
51 ppm or μ mol mol⁻¹) is measured by a fast-response gas analyser and the vertical wind velocity
52 w (in m s⁻¹) is often measured by a sonic anemometer. The prime denotes the fluctuations from
53 the mean, while the overbar indicates time average. Equation 2 does not rely on ΔfCO_2
54 measurements nor empirical parameters and assumptions of the gas properties (Wanninkhof,
55 2014). EC flux measurements can therefore be considered useful as an independent reference
56 for bulk air-sea CO₂ flux estimates. Furthermore, the typical temporal and spatial scales of EC
57 flux measurements are ca. hourly and 1-10 km². These scales are much smaller than the
58 temporal and spatial scales of alternative techniques for measuring gas transfer, e.g. by dual
59 tracer methods (daily and 1000 km²) (Nightingale et al., 2000; Ho et al., 2006). EC
60 measurements are thus potentially better-suited to capture variations in gas exchange due to
61 small-scale processes at the air-sea interface (Garbe et al., 2014).



62 The EC CO₂ flux method has developed and improved over time. Before 1990, EC was
63 successfully used to measure air-sea momentum and heat fluxes. EC air-sea CO₂ flux
64 measurements made during those times were unreasonably high (Jones and Smith, 1977;
65 Wesely et al., 1982; Smith and Jones, 1985; Broecker et al., 1986). After 1990, with the
66 development of the infrared gas analyser, EC became routinely used for terrestrial carbon cycle
67 research (Baldocchi et al., 2001). Development of the EC method was accompanied by
68 improvements in the flux uncertainty analysis, which was generally based on momentum, heat
69 and land-atmosphere gas flux measurements (Lenschow and Kristensen, 1985; Businger, 1986;
70 Lenschow et al., 1994; Wienhold et al., 1995; Mahrt, 1998; Finkelstein and Sims, 2001;
71 Loescher et al., 2006; Rannik et al., 2009, 2016; Billesbach, 2011; Mauder et al., 2013;
72 Langford et al., 2015; Post et al., 2015).

73 In the late 1990s, the advancement in motion correction of wind measurements (Edson et al.,
74 1998; Yelland et al., 1998) facilitated ship-based EC CO₂ flux measurements from a moving
75 platform (McGillis et al., 2001; 2004). After 2000, a commercial open-path infrared gas
76 analyser LI-7500 became widely used for air-sea CO₂ flux measurements (Weiss et al., 2007;
77 Kondo and Tsukamoto, 2007; Prytherch et al., 2010; Edson et al., 2011; Else et al., 2011;
78 Lauvset et al., 2011). The LI-7500 generated extremely large and highly variable CO₂ fluxes
79 in comparison to expected (Kondo and Tsukamoto, 2007; Prytherch et al., 2010; Edson et al.,
80 2011; Else et al., 2011; Lauvset et al., 2011), which are generally considered to be an artefact
81 caused by water vapour cross-sensitivity (Kohsiek, 2000; Prytherch et al., 2010; Edson et al.,
82 2011; Landwehr et al., 2014). Mathematical corrections proposed to address this artefact
83 (Edson et al., 2011; Prytherch et al., 2010) were later shown to be unsatisfactory (Else et al.,
84 2011; Ikawa et al., 2013; Blomquist et al., 2014; Tsukamoto et al., 2014) or incorrect
85 (Landwehr et al., 2014).

86 The most reliable method for measuring EC air-sea CO₂ fluxes involves physical removal of
87 water vapour fluctuations from the sampled air. The simplest approach is to combine a closed-
88 path gas analyser with a physical dryer to eliminate most of the water vapour fluctuation (Miller
89 et al., 2010; Blomquist et al., 2014; Landwehr et al., 2014; Yang et al., 2016; Nilsson et al.,
90 2018). The tuneable-diode-laser-based cavity ring-down spectrometer (CRDS) made by
91 Picarro Inc. (Santa Clara, California, USA) is the most precise closed-path analyser currently
92 available (Blomquist et al., 2014). The closed-path infrared gas analyser LI-7200 (LI-COR
93 Biosciences, Lincoln, Nebraska, USA) is another popular choice.



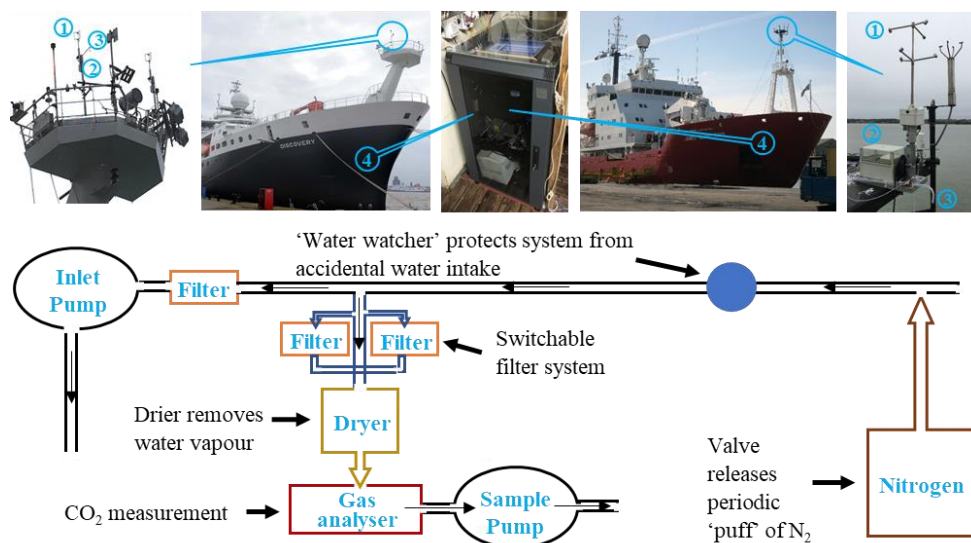
94 The advancements in instrumentation and in motion correction methods have significantly
95 improved the quality of air-sea EC CO₂ flux observations but, despite these changes, the flux
96 uncertainties have not been well-quantified. The aims of this study are to: 1) analyse
97 uncertainties in EC air-sea CO₂ flux measurements; 2) propose practical methods to reduce the
98 systematic and random flux uncertainty; and 3) investigate how the EC flux uncertainty
99 influences our ability to estimate and parameterise K_{660} .

100

101 2 Experiment and methods

102 2.1 Instrumental set-up

103



104

105 **Figure 1.** EC system (upper panel) and a diagram of system setup (bottom panel). EC instruments: 1)
106 Sonic anemometer, 2) Motion sensor, 3) Air sample inlet for gas analyser, 4) Datalogger/gas analyser.
107 Arctic and Atlantic data from 2018 were collected on the RRS James Clark Ross (JCR, upper right)
108 using a Picarro G2311-f, and Atlantic data from 2019 were collected using a LI-7200 on the RRS
109 Discovery (upper left).

110

111 The basic information of four cruises is summarised in Table 1. Appendix A shows the four
112 cruise tracks (Fig. A1, A2). Data from the Atlantic cruises (AMT28 and AMT29) are limited to



113 3° N–20° S in order to focus specifically on the performance of two different gas analysers in the
114 same region with low flux signal (tropical zone).

115

116 **Table 1.** Basic information for all four cruises on the RRS James Clark Ross (JCR) and RRS Discovery
117 that measured air-sea EC CO₂ fluxes.

Cruise	JR18006	JR18007	AMT28	AMT29
Data period	30 June–1 August 2019	5 August–29 September 2019	9 October–16 October 2018	4 November–11 November 2019
Visited region	Arctic Ocean (Barents Sea)	Arctic Ocean (Fram Strait)	Tropical Atlantic Ocean	Tropical Atlantic Ocean
Research vessel	JCR	JCR	JCR	Discovery
Gas analyser	Picarro G2311-f	Picarro G2311-f	Picarro G2311-f	LI-7200

118

119 The CO₂ flux and data logging systems installed on the JCR and Discovery were operated
120 autonomously. The EC systems were approximately 20 m above mean sea level on both ships
121 (at the top of the foremasts, Fig. 1) to minimise flow distortion and exposure to sea spray.
122 Computational fluid dynamics (CFD) simulation indicates that the airflow distortion at the top
123 of the JCR foremast is small (~1% of the free stream wind speed when the ship is head to wind,
124 Moat and Yelland, 2015). The hull structure of RRS Discovery is nearly identical to that of
125 RRS James Cook. CFD simulation of the James Cook indicates that the airflow at the top
126 foremast is distorted by ~2% for bow-on flows (Moat et al., 2006).

127 The EC system on the JCR consists of a three-dimensional sonic anemometer (Metek Inc.,
128 Sonic-3 Scientific), a motion sensor (initially Systron Donner Motionpak II, which compared
129 favourably with and was then replaced by a Life Performance-Research LPMS-RS232AL2 in
130 April 2019), and a Picarro G2311-f gas analyser. All instruments sampled at a frequency of 10
131 Hz or greater and the data were logged at 10 Hz with a datalogger (CR6, Campbell Scientific,
132 Inc.), similar to the setup by Butterworth and Miller (2016). Air is pulled through a long tube
133 (30 m, 0.95 cm inner diameter) with a dry vane pump at a flow rate of ~40 L min⁻¹ (Gast 1023
134 series). The Picarro gas analyser subsamples from this tube through a particle filter (Swagelok
135 2 µm) and a dryer (Nafion PD-200T-24M) at a flow of ~5 L min⁻¹ (Fig. 1). The dryer is setup
136 in the ‘re-flux’ configuration and uses the lower pressure Picarro exhaust to dry the sample air.
137 This method removes ~80% of the water vapour and essentially all of the humidity fluctuations



138 (Yang et al., 2016). The Picarro internal calculation accounts for the detected residual water
139 vapour and yields a dry CO₂ mixing ratio that is used in the flux calculations. A valve controlled
140 by the Picarro instrument injects a ‘puff’ of nitrogen (N₂) into the tip of the inlet tube for 30 s
141 every 6 hours. This enables estimates of the time delay and high-frequency signal attenuation
142 (Sect. 2.2).

143 The EC system on RRS Discovery consists of a Gill R3-50 sonic anemometer, a LPMS motion
144 sensor package, and a LI-7200 gas analyser. The LI-7200 gas analyser was mounted within the
145 enclosed staircase, directly underneath the meteorological platform and close to the inlet (inlet
146 length 7.5 m). A single pump (Gast 1023) was sufficient to pull air through a particle filter
147 (Swagelok 2 μm), a dryer (Nafion PD-200T-24M), and the LI-7200 at a flow of ~7 L min⁻¹.
148 There was no N₂ puff system setup on Discovery but equivalent lab tests confirmed that the
149 delay time was less than on the JCR because of the shorter inlet line. The dryer on the Discovery
150 is setup in the same ‘re-flux’ configuration as the JCR and uses the lower pressure at the LI-
151 7200 exhaust (limited by an additional 0.08 cm diameter critical orifice) to dry the sample air.
152 This setup removes ~60–70% of the water vapour and essentially all of the humidity
153 fluctuations. The dry CO₂ mixing ratio, computed by accounting for the LI-7200 temperature,
154 pressure and residual water vapour measurements, is used in the flux calculations.

155

156 **2.2 Flux processing**

157 The EC air-sea CO₂ flux calculation steps using the raw data are outlined with a flow chart
158 (Fig. 2) and detailed below. The raw high frequency wind and CO₂ data are processed first,
159 yielding fluxes in 20 min averaging time interval and related statistics. These statistics are then
160 used for quality control of the fluxes. Further averaging of the quality-controlled 20 min fluxes
161 to hourly or longer time scales is then used to reduce random error (Sect. 4.1). Linear
162 detrending was used to identify the turbulent fluctuations (i.e. w' and c') throughout the
163 analyses.

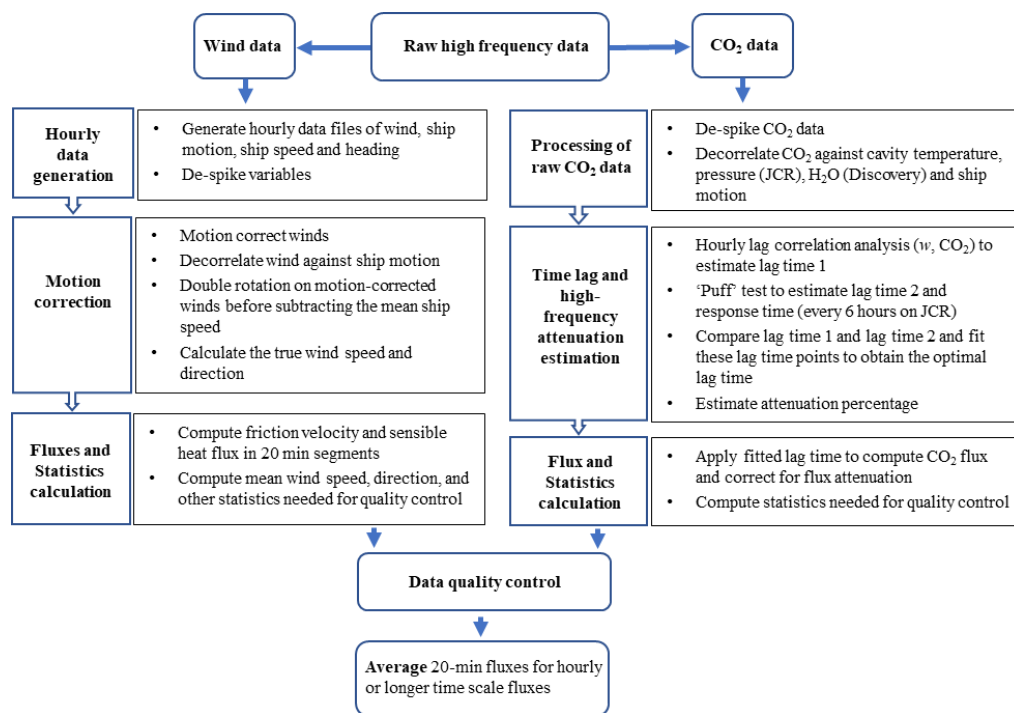
164 To correct the wind data for ship motion, we first generated hourly data files containing the
165 measurements from the sonic anemometer (three-dimensional wind speed components: u , v
166 and w and sonic temperature T_s), motion sensor (three axis accelerations: $accel_x$, $accel_y$,
167 $accel_z$; and rotation angles: rot_x , rot_y , rot_z), ship heading over ground (HDG, from the
168 gyro compass) and ship speed over ground (SOG, from Global Position System). Spikes larger
169 than 4 standard deviations (SDs) from the median were removed. Secondly, a complementary
170 filtering method using Euler angles (see Edson et al., 1998) was applied to the hourly data files



171 to remove apparent winds generated by the ship movements. The motion-corrected winds were
172 further decorrelated against ship motion to remove any residual motion-sensitivity (Miller et
173 al., 2010; Yang et al., 2013). The motion-corrected winds were double rotated to account for
174 the wind streamline over the ship, yielding the vertical wind velocity (w) required in Eq. 2.
175 Inspection of frequency spectra showed that the spectral peak at the ship motion frequencies
176 (approximately 0.1–0.3 Hz) had disappeared after the motion correction (Fig. S1, Supplement).
177 This indicates that the majority of ship motion had been removed from the measured wind
178 speed. The last step in the wind data processing was the calculation of 20 min average friction
179 velocity, sensible heat flux and other key variables used for data quality control (Table S1,
180 Supplement).

181 The CO₂ data were de-spiked (by removing values > 4 SDs from the median). The Picarro CO₂
182 mixing ratio was further decorrelated against analyser cell pressure and temperature to remove
183 CO₂ variations due to ship's motion. The LI-7200 CO₂ mixing ratio was further decorrelated
184 against the LI-7200 H₂O mixing ratio and temperature to remove residual air density
185 fluctuations, following Landwehr et al. (2018). CO₂ data were also decorrelated against ship's
186 heave and accelerations because these can produce spurious CO₂ variability (Miller et al., 2010;
187 Blomquist et al., 2014).

188 A lag between CO₂ data acquisition and the wind data is created because of the time taken for
189 sample air to travel through the inlet tube. On the JCR, we use the 'puff' system where the lag
190 time is the time difference between the N₂ 'puff' start (when the on/off valve is switched) and
191 the time when the diluted signal is sensed by the gas analyser. The lag time can also be
192 estimated by the maximum covariance method, calculated by shifting the time base of the CO₂
193 signal and finding the shift that achieves maximum covariance between the vertical wind
194 velocity (w) signal and the shifted CO₂ signal. The lag times estimated by the maximum
195 covariance method agree well with the estimates of the 'puff' procedure (Fig. S2, Supplement).
196 These estimates indicate a lag time of 3.3–3.4 s for the Arctic cruises and 3.3 s for cruise
197 AMT28 on the JCR. The maximum covariance method estimated lag time on Discovery
198 (AMT29) was 2.6 s, consistent with laboratory test results prior to the cruise.



199

200 **Figure 2.** Flow chart of EC data processing. The raw high frequency (10 Hz) wind and CO₂ data were
 201 initially processed separately and then combined to calculate fluxes. CO₂ fluxes were filtered by a series
 202 of data quality control criteria. The 20-min flux intervals were averaged to longer time scales (hourly
 203 or more). The data processing is detailed in the text.

204

205 The inlet tube, particle filter and dryer cause high-frequency CO₂ flux signal attenuation. The
 206 N₂ ‘puff’ was also used to assess the response time by considering the e-folding time in the
 207 CO₂ signal change (similar approaches have been used by Bariteau et al., 2010; Blomquist et
 208 al., 2014, Bell et al., 2015). The response time is 0.35 s for the EC system on JCR and 0.25 s
 209 for the EC system on Discovery (estimated in the laboratory prior to cruise). These response
 210 times were combined with the relative wind speed-dependent, theoretical shapes of the
 211 cospectra (Kaimal et al., 1972) to estimate the percentage flux loss due to the inlet attenuation
 212 (Yang et al., 2013). The mean attenuation percentage is less than 10% with a relative wind
 213 speed dependence (Fig. S3, Supplement). The attenuation percentage value was applied to the
 214 computed flux to compensate the flux loss due to the high-frequency signal attenuation. Finally,
 215 horizontal CO₂ fluxes and other statistics such as CO₂ range and CO₂ trend were computed for
 216 quality control purposes (Table S1, Supplement).



217 The computed 20-min fluxes were filtered for non-ideal ship manoeuvres or violations of the
218 homogeneity/stationary requirement of EC (see Supplement for the quality control criteria).

219

220 2.3 Uncertainty analysis methods

221 2.3.1 Uncertainty components

222 Uncertainty contains two components: systematic error (δF_S) and random error (δF_R).
223 According to propagation of uncertainty theory (JCGM, 2008), the total uncertainty in EC CO₂
224 fluxes (from random and systematic errors) can be expressed as:

$$225 \quad \delta F = \sqrt{\delta F_R^2 + \delta F_S^2} \quad (3)$$

226 Systematic errors (Sect. 2.3.2) will cause bias in the flux. They thus should be
227 eliminated/minimised with appropriate system setup and, if needed, effective numerical
228 corrections. Random error results in imprecision (but not bias) and can be reduced by averaging
229 repeated measurements (Sect. 2.3.3). Errors due to insufficient sampling and instrument noise
230 are generally considered most important in EC flux measurements (Lenschow and Kristensen,
231 1985; Businger 1986; Mauder et al., 2013; Rannik et al., 2016).

232 Sampling error is an inherent issue for EC flux measurements and is typically the main source
233 of the CO₂ flux uncertainty (Mauder et al., 2013). The sampling error is caused by the
234 difference between the ensemble average and the time average. The calculation of EC flux (Eq.
235 2) requires the separation between the mean and fluctuating components, which can be
236 represented fully for CO₂ mixing ratio c as:

$$237 \quad c(x, t) = \bar{c}(x, t) + c'(x, t) \quad (4)$$

238 The mean component \bar{c} represents ensemble average over time (t) and space (x) and does not
239 contribute to the flux. The time average of a stationary turbulent signal and space average of a
240 homogenous turbulent signal theoretically converge on the ensemble average when the
241 averaging time approaches infinity, i.e. $T \rightarrow \infty$ (Wyngaard, 2010). In practice, Reynolds
242 averaging over a much shorter time interval (10 min to an hour) is typically used for EC flux
243 measurements from a fixed point or from a slow-moving platform such as a ship. This is
244 because the atmospheric boundary layer is only quasi-stationary for a few hours. Non-
245 stationarity (e.g. diurnal variability and synoptic conditions) is an inherent property of the



246 atmospheric boundary layer (Wyngaard, 2010). EC flux observations thus inevitably contain
247 some random error due to insufficient sampling time, and this error is greater at shorter
248 averaging times.

249 Random error due to instrument noise comes mainly from the white noise of the gas analyser,
250 as the noise from the sonic anemometer is relatively unimportant (Blomquist et al., 2010;
251 Fairall et al., 2000; Mauder et al., 2013). Blomquist et al. (2014) show ‘pink’ noise with a weak
252 spectral slope for their CRDS gas analyser (G1301-f), but the gas analysers on JCR (G2311-f)
253 and Discovery (LI-7200) demonstrate white noise with a constant variance at high frequency
254 (Fig. B2, Appendix B).

255

256 2.3.2 Systematic error

257 Table 2 details the measures taken during instrument setup and data processing that help
258 eliminate most sources of systematic error in EC CO₂ fluxes.

259

260 **Table 2.** Potential sources of bias in our EC air-sea CO₂ flux measurements and the methods used to
261 minimise them.

Potential source of bias	Methods used to minimise the bias	Flux uncertainty
$\delta F_{S,1}$ Water vapour cross-sensitivity	Closed-path gas analyser with a dryer removes essentially all of the water vapour fluctuation (Blomquist et al., 2014; Yang et al., 2016). The residual H ₂ O signal is measured by the gas analyser and used in the calculation of dry CO ₂ mixing ratio, which removes water cross-sensitivity.	Negligible
$\delta F_{S,2}$ Ship motion	Flux uncertainty from an earlier version of the motion correction procedure (less rigorous than the one used by ourselves) is estimated to be 10-20% (Edson et al. 1998). The more recently-adopted decorrelation of vertical winds and CO ₂ against platform motion (Miller et al., 2010; Yang et al., 2013) reduces this uncertainty. Flügge et al. (2016) compare EC momentum fluxes measured from a moving platform (buoy) with fluxes measured from a nearby fixed tower. Flux estimates from these two platforms agree well (relative flux bias due to the motion correction $\leq 6\%$).	$\leq 6\%$



<p>$\delta F_{S,3}$ Airflow distortion</p>	<p>The EC flux system is deployed as far forward and as high as possible on the ship (top of the foremast), which minimises the impacts of flow distortion. Subsequent distortion correction using the CFD simulation (Moat et al., 2006; Moat and Yelland, 2015) along with a relative wind direction restriction further reduces the impact of flow distortion on the fluxes. Measured EC friction velocities and friction velocities from the COARE3.5 model (Edson et al., 2013) agree well (e.g. $R^2 = 0.95$, slope = 0.97) for data collected during cruise JR18006. Good comparison between observed and COARE3.5 friction velocity estimates indicates that we have fully accounted for flow distortion effects.</p>	<p>Negligible</p>
<p>$\delta F_{S,4}$ Inlet effects (high-frequency flux attenuation and CO₂ sampling delay)</p>	<p>High-frequency flux signal attenuation (in the inlet tube, particle filter and dryer) is evaluated by the CO₂ signal response to a puff of N₂ gas. Flux attenuation is calculated from the ‘inlet puff’ response and applied as a correction (< 10%, see Sect. 2.2). The uncertainty in the attenuation correction is about 1% for unstable/neutral atmospheric conditions, which is generally the case over the ocean (e.g. 93% of the time for the Atlantic cruises, 80% of the time for the Arctic cruises). During stable conditions, the attenuation correction is larger (Landwehr et al., 2018) and the uncertainty is also greater (~20%).</p> <p>The lag time adjustment prior to the flux calculation aligns the CO₂ and wind signals. Two methods are used to estimate the optimal lag time: puff injection and maximum covariance. The two lag estimates are in good agreement (Sect. 2.2). Random adjustment of ± 0.2 s (1 σ of the puff test result) to the optimal lag time impacts the CO₂ flux by < 1%.</p>	<p>< 2% for vast majority of the cruises</p>
<p>$\delta F_{S,5}$ Spatial separation between the sonic anemometer and the gas inlet</p>	<p>The CO₂ inlet is ~70 cm directly below the centre volume of the sonic anemometer. This distance is small relative to the size of the dominant flux-carrying eddies encountered by the EC measurement system height above sea level. The excellent agreement between the lag time determined by the puff system and by the optimal covariance method further confirms that the distance between the CO₂ inlet and anemometer is sufficiently small.</p>	<p>Negligible</p>



$\delta F_{S,6}$ Imperfect calibration of the sensors	The potential flux bias resulting from instrument calibration (gas analyser, anemometer and meteorological sensors required to calculate air density: air temperature, relative humidity and pressure) is up to 4% for the JCR setup. The largest instrument calibration uncertainty derives from the wind sensor accuracy ($\pm 0.15 \text{ m s}^{-1}$ at 4 m s^{-1} winds according to the Metek uSonic instrument specification). This bias is even lower ($< 2\%$) for the Discovery setup because the Gill R3 sonic anemometer is more accurate.	$\leq 4\%$
Propagated bias	Estimated from the individual bias estimates above ($\delta F_{S,1}, \delta F_{S,2}, \text{ etc.}$) using $\delta F_S = \sqrt{\sum_1^n \delta F_{S,n}^2}$	$< 7.5\%$

262

263 In addition to bias sources related to the instrument setup (Table 2), insufficient sampling time
 264 (an inherent issue of EC fluxes) may also generate a systematic error. We use a theoretical
 265 method to estimate this systematic error in EC CO₂ flux (Lenschow et al., 1994):

$$266 \quad |\delta F_S| \leq 2\sigma_w \sigma_{c_a} \frac{\sqrt{\tau_w \tau_c}}{T} \quad (5)$$

267 where σ_w (m s^{-1}) and σ_{c_a} (ppm) are the standard deviations of the vertical wind velocity and
 268 the CO₂ mixing ratio due to atmospheric processes, respectively. T is the averaging time
 269 interval (s), and τ_w and τ_c are integral time scales (s) for vertical wind velocity and CO₂ signal,
 270 respectively. The definition and estimation of the integral time scale are shown in Appendix B.
 271 The sign of δF_S could be positive or negative (i.e. under or over-estimation) because of the
 272 poor statistics in capturing low-frequency eddies within the flux averaging period (Lenschow
 273 et al., 1993). The mean hourly relative systematic error due to insufficient sampling time for
 274 four cruises estimated by Eq. 5 is $< 5\%$. According to propagation of uncertainty theory (JCGM,
 275 2008), the total systematic error is less than 9% ($= \sqrt{7.5\%^2 + 5\%^2}$).

276 2.3.3 Random error

277 Five approaches used to estimate the total random error (A-C) and the random error component
 278 due to instrument noise (C-E) in EC CO₂ fluxes are discussed below. The random error
 279 assessments are empirical (A and D) or theoretical (B, C and E).

280 **A.** An empirical approach to estimate total random error involves shifting the w data relative
 281 to the CO₂ data (or vice versa) by a large, unrealistic time shift and then computing the ‘null



282 fluxes' from the time-desynchronized CO₂ and *w* time series (Rannik et al., 2016). The shift
283 removes any real correlation between CO₂ and *w* due to vertical exchange. The standard
284 deviation of the resultant 'null' fluxes represents the random flux uncertainty (Wienhold et al.,
285 1995). We applied a series of time shifts of $\sim 20 - 60 \times \tau_w$ (i.e. using time shifts ranging from
286 -300 to -100 and 100 to 300 s, Rannik et al., 2016). This empirical estimation of total random
287 flux uncertainty will hereafter be referred to as $\delta F_{R,Wienhold}$.

288 **B.** Lenschow and Kristensen (1985) derived a rigorous theoretical equation for total random
289 error estimation, which contains both the auto-covariance and cross-covariance functions. The
290 theoretical equation has been numerically approximated by Finkelstein and Sims (2001):

$$291 \quad \delta F_{R,Finkelstein} = \left\{ \frac{1}{n} \left[\sum_{p=-m}^m r_{ww}(p) r_{cc}(p) + \sum_{p=-m}^m r_{wc}(p) r_{cw}(p) \right] \right\}^{1/2} \quad (6)$$

292 where *n* is the number of data points within an averaging time interval, *p* is the number of
293 shifting points. The maximum shifting point *m* can be chosen subjectively ($< n$). We found that
294 the random error for *m* between 1000 and 2000 data points was similar, so for this study we
295 use $m = 1500$ (150 s shift time). The first term in the brackets represents the auto-covariance
296 component and the second term is the cross-covariance component. r_{ww} and r_{cc} are the auto-
297 covariance functions for vertical wind velocity (*w*) and CO₂ mixing ratio (*c*), respectively. r_{wc}
298 and r_{cw} are the cross-covariance functions for *w* and *c*. Here r_{wc} represents shifting *w* data
299 relative to CO₂ data, while r_{cw} represents shifting CO₂ data relative to *w* data.

300 **C.** Blomquist et al. (2010) attributed the sources of CO₂ variance σ_c^2 to atmospheric processes
301 ($\sigma_{c_a}^2$) and white noise ($\sigma_{c_n}^2$). The sources of variance are considered to be independent of each
302 other and the sonic anemometer is assumed to be relatively noise-free. According to
303 propagation of uncertainty theory (JCGM, 2008), the total random flux error can be defined as:

$$304 \quad \delta F_{R,Blomquist} \leq \frac{a\sigma_w}{\sqrt{F}} \left(\sigma_{c_a}^2 \tau_{wc} + \sigma_{c_n}^2 \tau_{c_n} \right)^{1/2} \quad (7)$$

305 where the constant *a* varies from $\sqrt{2}$ to 2, depending on the relationship between the covariance
306 of the two variables (*w* and CO₂) and the product of their auto-correlations (Lenschow and
307 Kristensen, 1985). Here, τ_{wc} is equal to the shorter of τ_w and τ_c , which is typically τ_w
308 (Blomquist et al., 2010), and τ_{c_n} is the integral time scale of white noise in the CO₂ signal. The
309 CO₂ variance due to atmospheric processes ($\sigma_{c_a}^2$) includes two components: variance due to
310 vertical flux (i.e. air-sea CO₂ flux) $\sigma_{c_{av}}^2$, and variance due to other atmospheric processes $\sigma_{c_{ao}}^2$



311 (Fairall et al., 2000). The variance in CO₂ due to vertical flux ($\sigma_{c_{av}}^2$) depends on atmospheric
312 stability. $\sigma_{c_{av}}^2$ can be estimated with Monin-Obukhov similarity theory (Blomquist et al., 2010,
313 2014; Fairall et al., 2000):

$$314 \quad \sigma_{c_{av}}^2 = \left[3 \frac{\overline{w'c'}}{u_*} f_c(z/L) \right]^2 \quad (8)$$

315 where u_* is the friction velocity (m s⁻¹) and the similarity function (f_c) depends on the stability
316 parameter z/L , where z is the observational height (m) and L is the Obukhov length (m). The
317 expression of f_c can be found in Blomquist et al. (2010).

318 Equation 7 can be used to assess the random error due to instrument noise by setting $\sigma_{c_a}^2 = 0$,
319 referred to hereafter as $\delta F_{RN, Blomquist}$. We use the CO₂ variance spectra to directly estimate the
320 white noise term $\sigma_{c_n}^2 \tau_{c_n}$ in Eq. 7. The variance is fairly constant at high frequency (1-5 Hz; Fig.
321 B2, Appendix B), which is often referred to as band-limited white noise. The relationship
322 between $\sigma_{c_n}^2 \tau_{c_n}$ and the band-limited noise spectral value φ_{c_n} , is expressed in Blomquist et al.
323 (2010) as:

$$324 \quad \sigma_{c_n}^2 \tau_{c_n} = \frac{\varphi_{c_n}}{4} \quad (9)$$

325 **D.** Billesbach (2011) developed an empirical method to estimate the random error due to
326 instrument noise alone (referred to as $\Delta F_{RN, Billesbach}$). This involves random shuffling of the
327 CO₂ time series within an averaging interval and then calculating the covariance of w and CO₂.
328 The correlation between w and CO₂ is minimized by the shuffling, and any remaining
329 correlation between w and CO₂ is due to the unintentional correlations contributed by
330 instrument noise.

331 **E.** Mauder et al. (2013) describe another theoretical approach to estimate the random flux error
332 due to instrument noise:

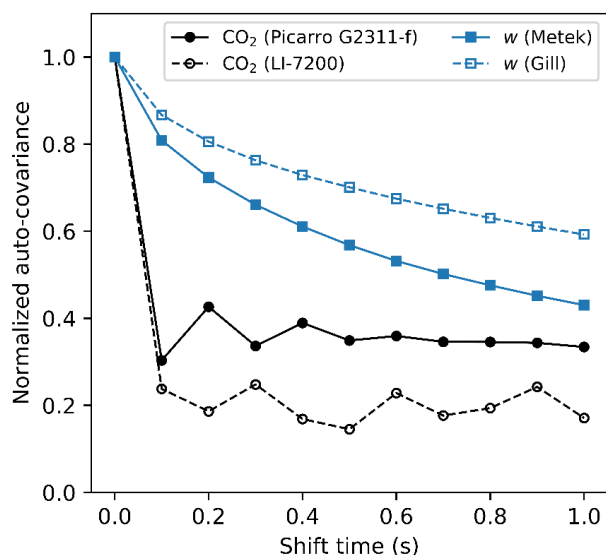
$$333 \quad \delta F_{RN, Mauder} = \frac{\sigma_w \sigma_{c_n}}{\sqrt{n}} \quad (10)$$

334 White noise correlates with itself but is uncorrelated with atmospheric turbulence. Thus, the
335 white noise-induced CO₂ variance (σ_{c_n}) only contributes to the total variance. The value of σ_{c_n}
336 can be estimated from the difference between the zero-shift auto-covariance value (CO₂
337 variance σ_c^2) and the noise-free variance extrapolated to a time shift of zero (Lenschow et al.,
338 2000):



339
$$\sigma_{c_n}^2 = \sigma_c^2 - \sigma^2(t \rightarrow 0) \quad (11)$$

340 where $\sigma^2(t \rightarrow 0)$ represents the extrapolation of auto-covariance to a zero shift, which is
341 considered equal to variance due to atmospheric processes ($\sigma_{c_a}^2$). Figure 3 shows the normalised
342 auto-covariance function curves of w and CO_2 as measured by the Picarro G2311-f and the LI-
343 7200. There is a sharp decrease in the CO_2 auto-covariance when shifting from 0 s shift to 0.1
344 s shift for both the Picarro G2311-f and LI-7200 gas analyser. The same sharp decrease is not
345 seen in the vertical wind velocity (w) auto-covariance. The relative difference in the change in
346 normalised auto-covariance shows that white noise makes a much larger relative contribution
347 to the CO_2 variance than to the vertical wind velocity variance.



348
349 **Figure 3.** Mean normalised auto-covariance functions of CO_2 and vertical wind velocity (w) by four
350 different instruments. The sharp decrease of the CO_2 auto-covariance between the zero shift and the
351 initial 0.1 s shift corresponds to the large contribution of white noise from the gas analysers. The LI-
352 7200 is the noisier instrument. The noise contribution from either anemometer is relatively small (<
353 10%).

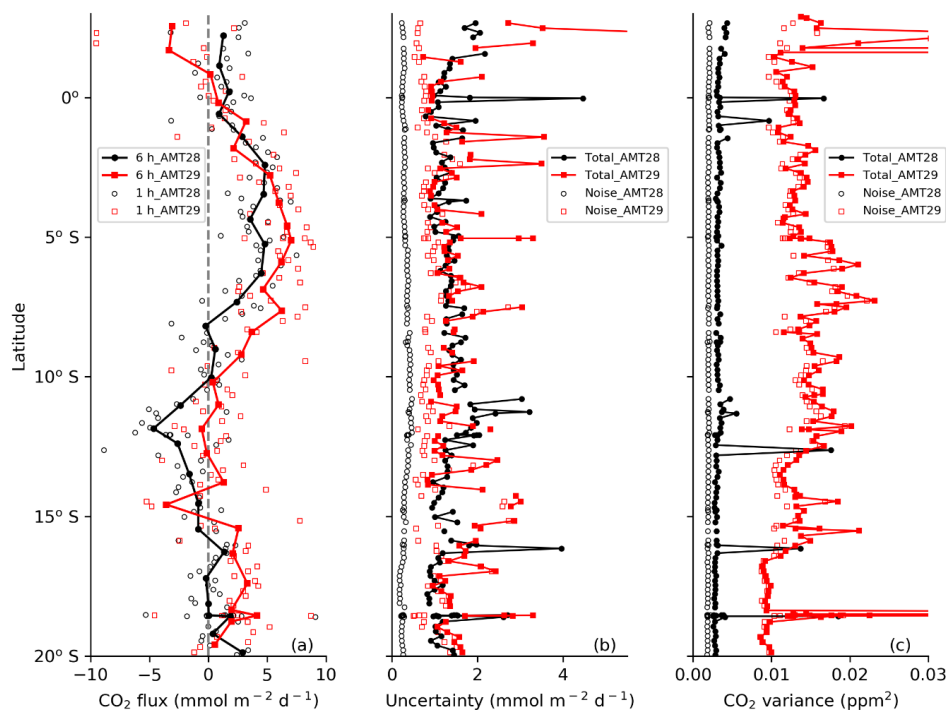
354

355 3 Results

356 Measurements from AMT28 and AMT29 set the scene for our uncertainty analysis. These two
357 Atlantic cruises transited across the same tropical region (Fig. A2, Appendix A) in October



358 2018 and September 2019 with different eddy covariance systems (Sect. 2.1). AMT28 and
359 AMT29 show broadly similar latitudinal patterns (Fig. 4a). An obvious question of interest is
360 whether the measured fluxes were the same for the two years. To answer this question, the
361 measurement uncertainties must be quantified. The total random uncertainties in CO₂ flux
362 ($\delta F_{R, \text{Finkelstein}}$) are comparable for the two cruises even though the random error component
363 due to instrument noise ($\delta F_{RN, \text{Mauder}}$) is about 3 times higher during AMT29 using LI-7200
364 than during AMT28 using Picarro G2311-f (Fig. 4b; Fig. D1, Appendix D). The similar total
365 random uncertainty in the AMT28 and AMT29 fluxes shows that both gas analysers are equally
366 suitable for air-sea EC CO₂ flux measurements. The variance budgets of atmospheric CO₂
367 mixing ratio (used to estimate random flux uncertainty, see Sect. 3.1) are shown in Fig. 4c.
368 Total variance in CO₂ mixing ratio is dominated by instrument noise on both cruises. CO₂
369 mixing ratio variance (total and instrument noise) was substantially higher during AMT29.



370

371 **Figure 4.** (a) Air-sea CO₂ fluxes (hourly and 6-h averages), (b) random uncertainty in flux (total and
372 due to instrument noise only), and (c) variance in CO₂ mixing ratio (total and due to instrument noise
373 only) for two Atlantic cruises.

374



375 3.1 Random uncertainty

376 Theoretical derivation of flux uncertainty ($\delta F_{RN, \text{Blomquist}}$, Eq. 7) requires knowledge of the
377 contributions to CO₂ mixing ratio variance. Total CO₂ variance is made up of instrument noise
378 ($\sigma_{c_n}^2$) and atmospheric processes ($\sigma_{c_a}^2$). Atmospheric processes include vertical flux ($\sigma_{c_{av}}^2$) and
379 other atmospheric processes ($\sigma_{c_{ao}}^2$). The variance budgets of CO₂ mixing ratio for the four
380 cruises are listed in Table 3. Atmospheric processes contribute a larger CO₂ variance in the
381 Arctic (where flux magnitudes are greater) compared to the Atlantic. Vertical flux accounts for
382 ~10% of the variance in CO₂ mixing ratio in the Arctic and ~1% of the CO₂ variance in the
383 Atlantic. Previous results demonstrate that horizontal transport is a major source of $\sigma_{c_{ao}}^2$ for
384 long-lived greenhouse gases (Blomquist et al., 2012). Small changes in CO₂ mixing ratio
385 transported horizontally can yield variance that greatly exceeds the variance from vertical flux.

386

387 **Table 3.** Variance in the CO₂ mixing ratio estimated using Eq. 8 and 11 for the Arctic (JR18006/7,
388 Picarro G2311-f) and Atlantic cruises (AMT28, Picarro G2311-f; AMT29, LI-7200). Total CO₂
389 variance (σ_c^2) consists of white noise ($\sigma_{c_n}^2$) and atmospheric processes ($\sigma_{c_a}^2$). The latter can be further
390 broken down to the CO₂ variance due to vertical flux ($\sigma_{c_{av}}^2$) and due to other processes ($\sigma_{c_{ao}}^2$).

CO ₂ variance ($\times 10^{-3}$ ppm ²)	JR18006	JR18007	AMT28	AMT29
Total, σ_c^2	9.9	8.6	3.6	13.9
Due to instrument white noise, $\sigma_{c_n}^2$	5.8	5.4	2.0	12.6
Due to atmospheric processes, $\sigma_{c_a}^2$	4.1	3.3	1.6	1.3
- Due to vertical flux, $\sigma_{c_{av}}^2$	1.3	0.8	0.03	0.08
- Due to other atmospheric processes, $\sigma_{c_{ao}}^2$	2.8	2.5	1.6	1.2

391

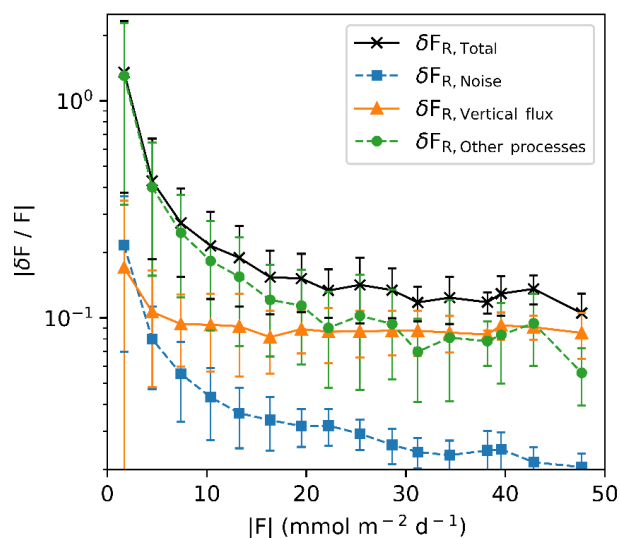
392 Three quasi-independent methods were used to estimate random uncertainty in EC air-sea CO₂
393 fluxes caused by instrument noise (δF_{RN} , Methods C-E, Sect. 2.3.3). Good agreement was
394 found between all three estimates (Fig. C2, Appendix C) when $\sqrt{2}$ is used as the constant in
395 Eq. 7 (a). The $\Delta F_{RN, \text{Billesbach}}$ estimates have more scatter and are slightly higher than the
396 theoretical results, possibly because the random shuffling of data fails to fully exclude the
397 contribution from atmospheric turbulence (Rannik et al., 2016). For the remainder of this study,
398 we use the $\delta F_{RN, \text{Mauder}}$ method to estimate δF_{RN} .

399 We used three methods to estimate the total random uncertainty (δF_R , Methods A-C, Sect. 2.3.3)
400 in the hourly-averaged air-sea CO₂ fluxes. There is good agreement among the three estimates



401 ($r > 0.88$; Fig. C1, Appendix C). Again, the constant in Eq. 7 (a) is set to $\sqrt{2}$, as informed by
402 the instrument noise uncertainty analysis above. We use $\delta F_{R, \text{Finkelstein}}$ (Eq. 6) to estimate the
403 total random flux uncertainty hereafter. Our decision is based on $\delta F_{R, \text{Finkelstein}}$ not requiring
404 the integral time scale (unlike $\delta F_{R, \text{Blomquist}}$) and showing less scatter than $\delta F_{R, \text{Wienhold}}$.

405 Figure 5 shows the different relative contributions to the random flux uncertainty for the Arctic
406 cruises (hourly average). Here the uncertainty is normalised by the flux magnitude and then
407 averaged into flux magnitude bins. When the flux magnitude is sufficiently large ($> 20 \text{ mmol}$
408 $\text{m}^{-2} \text{ day}^{-1}$), the total relative random uncertainty in flux asymptotes to about 15% and is driven
409 by variance associated with both vertical flux and other atmospheric processes. This estimate
410 is similar to uncertainties in air-sea fluxes of other well resolved (i.e. high signal-to-noise ratio)
411 variables (Fairall et al., 2000). At a lower flux magnitude, uncertainty due to atmospheric
412 processes other than vertical flux dominates the total random uncertainty. Uncertainty due to
413 the white noise from the Picarro G2311-f gas analyser is small.



414

415 **Figure 5.** Relative random uncertainty in hourly CO_2 flux and its contribution from noise, vertical flux
416 and other processes during two Arctic cruises. Relative random uncertainty data are binned into 3 mmol
417 $\text{m}^{-2} \text{ day}^{-1}$ flux magnitude bins (error bars represent 1 standard deviation).

418

419 3.2 Summary of systematic and random uncertainties



420 The total uncertainty δF in the hourly average EC CO₂ flux (estimated using Eq. 3) ranges
 421 from 1.4 to 3.2 mmol m⁻² day⁻¹ in the mean for the four cruises (Table 4). Our EC flux system
 422 setup was optimal and subsequent corrections have minimised any bias to < 9% (Sect. 2.3.2).
 423 Systematic error is on average much lower than random error (Table 4). This means the
 424 accuracy of the EC CO₂ flux measurements is very high, but the precision of hourly averaged
 425 EC CO₂ air-sea flux measurements is relatively low. In Sect. 4.1, we discuss how the precision
 426 can be improved by averaging the observed fluxes for longer.

427

428 **Table 4.** Summary of hourly average EC CO₂ fluxes and associated uncertainties in the mean for the
 429 four cruises (mmol m⁻² day⁻¹). Shown are the mean CO₂ flux magnitude ($\overline{|F|}$, mmol m⁻² day⁻¹), upper
 430 limitation of the total uncertainty (δF , Eq. 3), upper limitation of the absolute systematic error ($|\delta F_S|$,
 431 propagated from Table 2 and Eq. 5), and random error (δF_R , Eq. 6). The random error components are
 432 white noise (δF_{RN} , Eq. 10), vertical flux (δF_{RV} , Eq. 7) and other atmospheric processes ($\delta F_{RO} =$
 433 $\sqrt{\delta F_R^2 - \delta F_{RN}^2 - \delta F_{RV}^2}$). The total uncertainty is also expressed as a % of the mean flux magnitude
 434 ($\delta F/|F| \times 100\%$).

Cruises	JR18006	JR18007	AMT28	AMT29
$\overline{ \text{CO}_2 \text{ flux} }, \overline{ F }$	10.1	16.3	2.5	3.5
Total uncertainty, δF	2.3	3.2	1.4	1.7
($\delta F/ F \times 100\%$)	(23%)	(20%)	(58%)	(49%)
Systematic error, δF_S	0.8	1.2	0.3	0.3
Total random error, δF_R	2.2	2.9	1.4	1.7
Random error due to white noise, δF_{RN}	0.5	0.6	0.3	1.0
Random error due to vertical flux, δF_{RV}	1.1	1.4	0.2	0.4
Random error due to other atmospheric processes, δF_{RO}	1.5	2.4	1.4	1.5

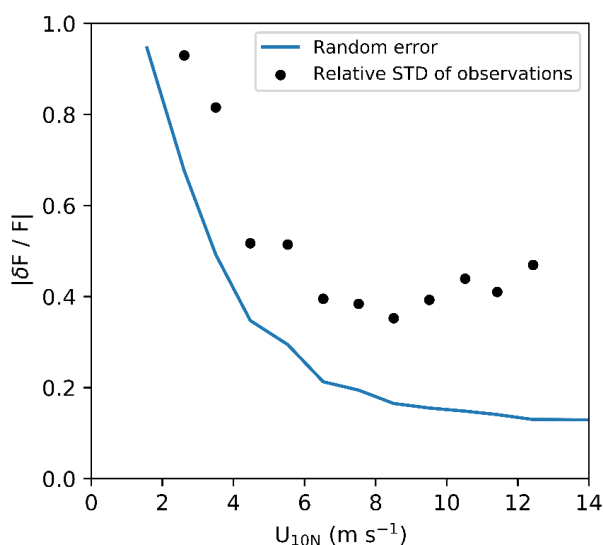
435

436 The theoretical uncertainty estimates above can be compared with a portion of the AMT28
 437 cruise data (15°–20° S, ~25° W; Fig. 4), when the ship encountered sea surface CO₂ fugacity
 438 close to equilibrium with the atmosphere (i.e. $\Delta f\text{CO}_2 \sim 0$, Fig. A2, Appendix A). The data from
 439 this region is useful for assessing the random and systematic flux uncertainties. The standard
 440 deviation of the EC CO₂ flux during cruise AMT28 when $\Delta f\text{CO}_2 \sim 0$ is 1.6 mmol m⁻² day⁻¹,
 441 which compares well with the theoretical random flux uncertainty in this region (1.4 mmol m⁻²
 442 day⁻¹). The mean EC CO₂ flux from this region was 0.5 mmol m⁻² day⁻¹, which is



443 indistinguishable from zero considering the random uncertainty. This further confirms the
444 minimal bias in our flux observations.

445 Figure 6 shows a comparison between the relative uncertainty and the relative standard
446 deviation (RSTD) in the hourly CO₂ flux for the two Arctic cruises. Results have been binned
447 into 1 m s⁻¹ wind speed bins. Wind speed was converted to 10-meter neutral wind speed (U_{10N})
448 using the COARE3.5 model (Edson et al., 2013). The relative random error decreases with
449 increasing wind speed. This is partly because the fluxes tend to be larger at higher wind speeds
450 and so the signal-to-noise ratio in the flux is greater. In addition, at higher wind speeds, a greater
451 number of high-frequency turbulent eddies are sampled by the EC system, providing better
452 statistics of turbulent eddies, and lower sampling error.



453

454 **Figure 6.** Comparison of relative random uncertainty in hourly CO₂ flux and relative standard
455 deviation (RSTD, standard deviation/|flux mean|) of the EC CO₂ flux from two Arctic cruises. These results
456 are binned in 1 m s⁻¹ wind speed bins.

457

458 The RSTD of the flux is greater in magnitude than the estimated flux uncertainty because it
459 also contains environmental variability. The CO₂ flux auto-covariance analysis (Sect. 4.1)
460 shows that random error in hourly flux explains ~20% of the flux variance on average for the
461 two Arctic cruises. This implies that the remaining variability in the EC flux (~80%) is due to
462 natural phenomena (e.g. changes in $\Delta f\text{CO}_2$, wind speed, etc). Similarly, substantial variability



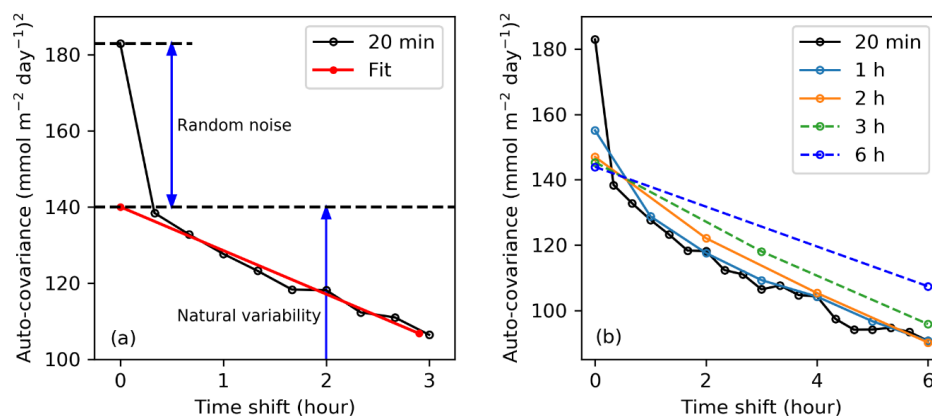
463 is typical in EC-derived CO₂ gas transfer velocity at a given wind speed (e.g. Edson et al., 2011;
464 Butterworth and Miller, 2016). K_{660} is derived from (EC CO₂ flux)/ Δf CO₂, and thus an
465 understanding of EC flux uncertainty can help understand and explain the variability in EC-
466 derived gas transfer velocity estimates (Sect. 4.2).

467 **4 Discussion**

468 **4.1 Impact of averaging time scale on flux uncertainty**

469 The random error in flux decreases with increasing averaging time interval T or the number of
470 sampling points n (Eq. 6, 7 and 10). This is because a longer averaging time interval results in
471 better statistics of the turbulent eddies. However, averaging for too long is also not ideal since
472 the atmosphere is less likely to maintain stationarity. The typical averaging time interval is thus
473 typically between 10 min and 60 min for air-sea flux measurements (20 min intervals were
474 used in this study). The timeseries of quality controlled 20 min flux intervals can be further
475 averaged over a longer time scale to reduce the random uncertainty. Averaging the 20 min flux
476 intervals assumes that the flux interval data are essentially repeat measurements within a
477 chosen averaging time scale. If the 20 min flux intervals are averaged, one can ask: What is the
478 optimal averaging time scale for interpreting air-sea EC CO₂ fluxes?

479 We use an auto-covariance method to determine the optimal averaging time scale. The observed
480 variance in CO₂ flux consists of random uncertainty (random noise) as well as natural
481 variability. The random noise component should only contribute to the CO₂ flux variance when
482 the data are zero-shifted. After the CO₂ flux data are shifted, the noise will not contribute to the
483 auto-covariance function. Figure 7 shows the auto-covariance function of the air-sea CO₂ flux
484 with different averaging time scales for Arctic cruise JR18007. For the 20-min fluxes (Fig. 7a),
485 the auto-covariance decreases rapidly between the zero shift and the initial time shift, which
486 indicates that a large fraction of the 20-min flux variance is due to random noise.



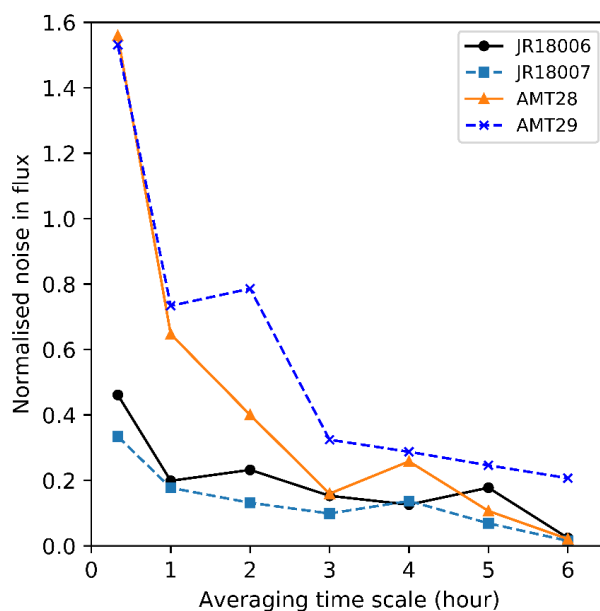
487

488 **Figure 7.** (a) Auto-covariance of the original 20-min fluxes (cruise JR18007) and a fit to the noise-free
489 auto-covariance function extrapolated back to a zero time shift. (b) CO₂ flux auto-covariance functions
490 with different averaging time scales. The black line represents the auto-covariance of the original 20-
491 min fluxes. The 20-min fluxes are further averaged at different time scales (1, 2, 3 and 6 hour) and the
492 corresponding auto-covariance functions are shown with different colours (dark blue, orange, green and
493 light blue).

494

495 The random noise in the CO₂ fluxes decreases with a longer averaging time scale, with the
496 greatest effect observed from 20 min to 1 hour (Fig. 7b). A fit to the noise-free auto-covariance
497 function extrapolated back to a zero time shift gives us an estimate of the non-noise variability
498 in the natural CO₂ flux. Subtracting the extrapolated natural flux variability from the total
499 variance in CO₂ flux provides an estimate of the random noise in the flux for each averaging
500 timescale (Fig. 7a). All four cruises consistently demonstrate a non-linear reduction in the noise
501 contribution to the flux measurements when the averaging timescale increases (Fig. 8). The
502 random noise in flux can be expressed relative to the natural variance in flux representing the
503 inverse of the signal-to-noise ratio (i.e. random noise in flux/natural flux variability ,
504 hereafter referred to as noise: signal).

505



506

507 **Figure 8.** Effect of the averaging timescale on the noise: signal (random noise in flux/
508 natural flux variability) for EC air-sea CO₂ flux measurements during four cruises.

509

510 The noise: signal also facilitates comparison of all four cruises (Fig. 8) and demonstrates the
511 consistent effect that increasing the averaging timescale has on noise: signal. Consistent with
512 Table 4, the Arctic cruises show much lower noise: signal because the flux magnitudes are
513 much larger. Typical detection limits in analytical science are often defined by a 1: 3 noise:
514 signal ratio. A 1: 3 noise: signal is achieved with a 1 h averaging timescale for the Arctic cruises.
515 The Atlantic cruises encountered much lower air-sea CO₂ fluxes and an averaging timescale of
516 at least 3 h is required to achieve the same 1: 3 noise: signal ratio.

517 The flux measurement uncertainty at a 6-h averaging timescale for the AMT cruises is ~0.6
518 mmol m⁻² day⁻¹. The analysis presented above permits an answer to the question posed at the
519 beginning of the Results section. The mean difference between the 6-h averaged EC CO₂ flux
520 observations on AMT29 and AMT28 (1.3 mmol m⁻² day⁻¹, Fig. 4a) is much greater than the
521 measurement uncertainty. This significant difference was likely because of the interannual
522 variability in AMT CO₂ flux due to changes in the natural environment (e.g. ΔfCO₂, sea surface
523 temperature, and physical drivers of interfacial turbulence such as wind speed) during the two
524 cruises.



525 At a typical research ship speed of ~ 10 knots, the AMT cruises cover ~ 110 km in 6 h, which is
526 equivalent to $\sim 1^\circ$ latitude. Averaging for longer than 6 h is likely to cause substantial loss of
527 real information about the natural variations in air-sea CO_2 flux and the drivers of flux
528 variability. For example, the mean flux between $0\text{--}20^\circ$ S during cruise AMT28 is 0.9 mmol m^{-2}
529 day^{-1} . However, the 6 h average EC measurements show that the flux varied between $+5 \text{ mmol}$
530 $\text{m}^{-2} \text{ day}^{-1}$ ($\sim 2\text{--}6^\circ$ S) and $-5 \text{ mmol m}^{-2} \text{ day}^{-1}$ ($\sim 11\text{--}13^\circ$ S, Fig. 4a).

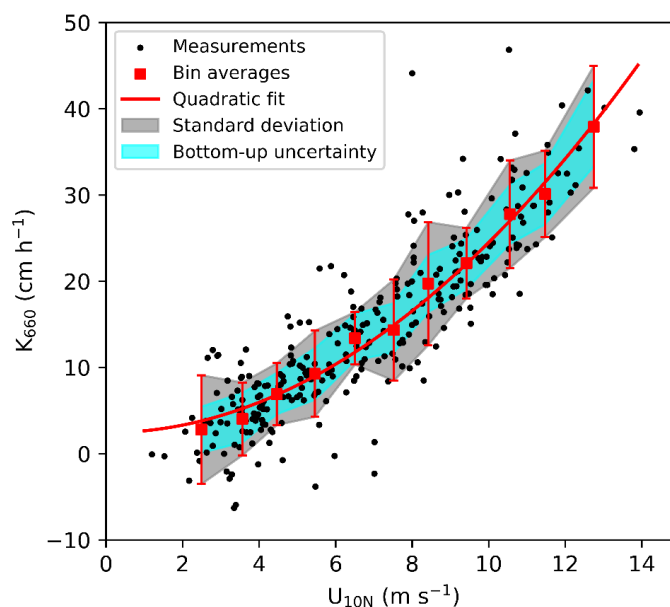
531

532 **4.2 Effect of CO_2 flux uncertainty on the gas transfer velocity K**

533 The uncertainties in the EC CO_2 air-sea flux measurement will influence the uncertainty that
534 translates to EC-based estimates of the gas transfer velocity, K . For illustration, K is computed
535 for Arctic cruise JR18007, which had a high flux signal: noise ratio of ~ 5 (Fig. 8). Any data
536 potentially influenced by ice and sea ice melt were excluded using a sea surface salinity filter
537 (data excluded when salinity < 32). Equation 1 is rearranged and used with concurrent
538 measurements of CO_2 flux (F), $\Delta f\text{CO}_2$, and sea surface temperature (SST) to obtain K adjusted
539 for the effect of temperature (K_{660}).

540 The determination coefficient (R^2) of the quadratic fit between wind speed ($U_{10\text{N}}$) and EC-
541 derived K_{660} (Fig. 9) demonstrates that wind speed explains 76% of the K_{660} variance during
542 Arctic cruise JR18007. How much of the remaining 24% can be attributed to uncertainties in
543 EC CO_2 fluxes?

544



545

546 **Figure 9.** Gas transfer velocity (K_{660}) measured on Arctic cruise JR18007 (hourly average, signal: noise
547 ~ 5) versus 10-m neutral wind speed (U_{10N}). Red squares represent 1 m s^{-1} bin averages with error bars
548 representing one standard deviation (SD). The red curve represents a quadratic fit using the bin averages:
549 $K_{660} = 0.22U_{10N}^2 + 2.46$ ($R^2 = 0.76$). The grey shaded area represents the standard deviation calculated
550 for each wind speed bin ($K_{660} \pm 1\text{SD}$). The cyan region represents the upper and lower bounds in K_{660}
551 uncertainty computed from the EC flux uncertainty ($K_{660} \pm \delta K_{660}$, see text for detail).

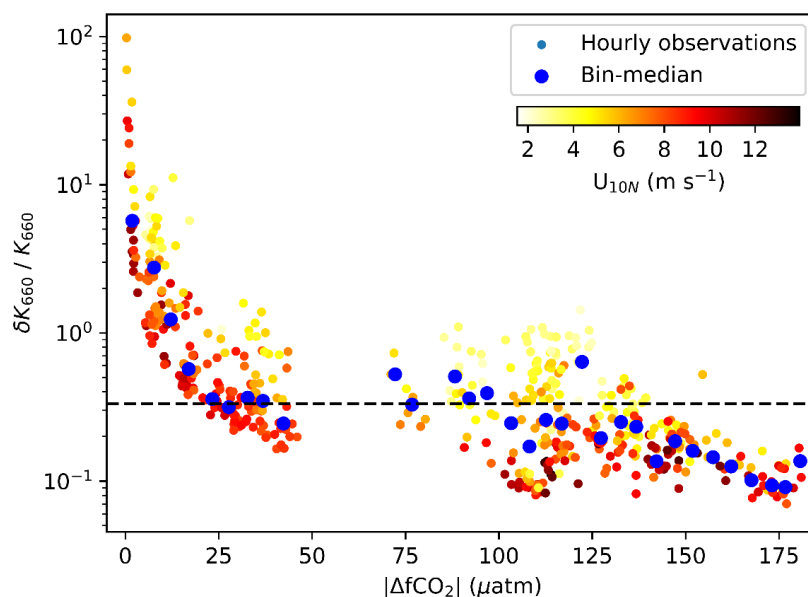
552

553 Variability in K_{660} within each 1 m s^{-1} wind speed bin can be considered to have minimal wind
554 speed influence. It is thus useful to compare the variability within each wind speed bin ($K_{660} \pm$
555 1SD) with the upper and lower uncertainty bounds derived from the EC flux measurements.
556 Uncertainty in EC flux-derived K_{660} (δK_{660}) is calculated from the uncertainty in hourly EC
557 flux (δF) by rearranging Eq. 1 (bulk flux equation) and replacing F with δF . The resultant δK_{660}
558 is then averaged in wind speed bins. The shaded cyan band in Fig. 9 ($K_{660} \pm \delta K_{660}$) is
559 consistently narrower than the grey shaded band ($K_{660} \pm 1\text{SD}$). On average, EC flux-derived
560 uncertainty in K_{660} can only account for a quarter of the K_{660} variance within each wind speed
561 bin and the remaining variance is most likely due to the non-wind speed factors that influence
562 gas exchange (e.g. breaking waves, surfactants).



563 The analysis above can be extended to assess how EC flux-derived uncertainty affects our
564 ability to parameterise K_{660} (e.g. as function of wind speed). To do so, a set of synthetic K_{660}
565 data is generated (same U_{10N} as the K_{660} measurements in Fig. 9). The synthetic K_{660} data are
566 initialised using a quadratic wind speed dependence that matches JR18007 (i.e. $K_{660} =$
567 $0.22U_{10N}^2 + 2.46$). Random Gaussian noise is then added to the synthetic K_{660} data, with relative
568 noise level corresponding to the relative flux uncertainty values taken from JR18007 (mean of
569 20%, Table 4). The relative uncertainty in K_{660} due to EC flux uncertainty ($\delta K_{660}/K_{660}$) shows
570 a wind speed dependence (Fig. S4a, Supplement), and the artificially-generated Gaussian noise
571 incorporates this wind speed dependence (Fig. S4b, Supplement). The R^2 of the quadratic fit to
572 the synthetic data as a function of U_{10N} is 0.90 (the rest of the variance is due to uncertainty in
573 K_{660}). Since wind speed explains 76% of variance in the observed K_{660} , it can be inferred that
574 non-wind speed factors can account for 14% (i.e. $(100-76)\% - (100-90)\%$) of the total variance
575 in K_{660} from this Arctic cruise. If the synthetic K_{660} data is assigned a relative flux uncertainty
576 of 50% (reflective of a region with low fluxes, e.g. AMT28/29), the R^2 of the wind speed
577 dependence in the synthetic data decreases to 0.60.

578 The relative uncertainty in EC flux-derived K_{660} ($\delta K_{660}/K_{660}$) is large when $|\Delta fCO_2|$ is small
579 (Fig. 10). Previous EC studies have filtered EC flux data to remove fluxes when the $|\Delta fCO_2|$
580 falls below a specified threshold (e.g. 20 μatm , Blomquist et al. (2017); 40 μatm , Miller et al.
581 (2010), Landwehr et al. (2014), Butterworth and Miller (2016), Prytherch et al. (2017); 50 μatm ,
582 Landwehr et al. (2018)). Analysis of the data presented here suggests that a $|\Delta fCO_2|$ threshold
583 of at least 20 μatm is reasonable for hourly K_{660} measurements, leading to δK_{660} of $\sim 10 \text{ cm h}^{-1}$
584 ($\delta K_{660}/K_{660} \sim 1/3$) or less on average. At very large $|\Delta fCO_2|$ of over 100 μatm , δK_{660} is reduced
585 to only a few cm h^{-1} ($\delta K_{660}/K_{660} \sim 1/5$). At longer flux averaging time scales, it may be possible
586 to relax the minimal $|\Delta fCO_2|$ threshold.



587

588 **Figure 10.** Relative uncertainty in EC-estimated hourly K_{660} ($\delta K_{660}/K_{660}$) versus the magnitude of the
589 air-sea CO_2 fugacity difference ($|\Delta f\text{CO}_2|$) during Arctic cruise JR18007 and Atlantic cruises AMT28
590 and AMT29 (no $\Delta f\text{CO}_2$ data were collected on JR18006). The data points are colour-coded by wind
591 speed. Blue points are medians of $\delta K_{660}/K_{660}$ in $5 \mu\text{atm}$ bins. Here we use the parameterised K_{660} (=
592 $0.22U_{10N}^2 + 2.46$) to normalise the uncertainty in K_{660} . The dashed line represents the 3: 1 signal: noise
593 ratio ($\delta K_{660}/K_{660} = 1/3$).

594

595 5. Conclusions

596 This study uses data from four cruises with a range in air-sea CO_2 flux magnitude to
597 comprehensively assess the sources of uncertainty in EC air-sea CO_2 flux measurements. Data
598 from two ships and two different state-of-the-art CO_2 analysers (Picarro G2311-f and LI-7200,
599 both fitted with a dryer) are analysed using multiple methods (Sect. 2.3). Random error
600 accounts for the majority of the flux uncertainty, while the systematic error (bias) is small
601 (Table 4). Random flux uncertainty is primarily caused by variance in CO_2 mixing ratio due to
602 atmospheric processes. The random error due to instrument noise for the Picarro G2311-f is
603 threefold smaller than for LI-7200 (Table 4 and Fig. D1, Appendix D). However, the
604 contribution of the instrument noise to the total random uncertainty is much smaller than the



605 contribution of atmospheric processes such that both gas analysers are well suited for air-sea
606 CO₂ flux measurements.

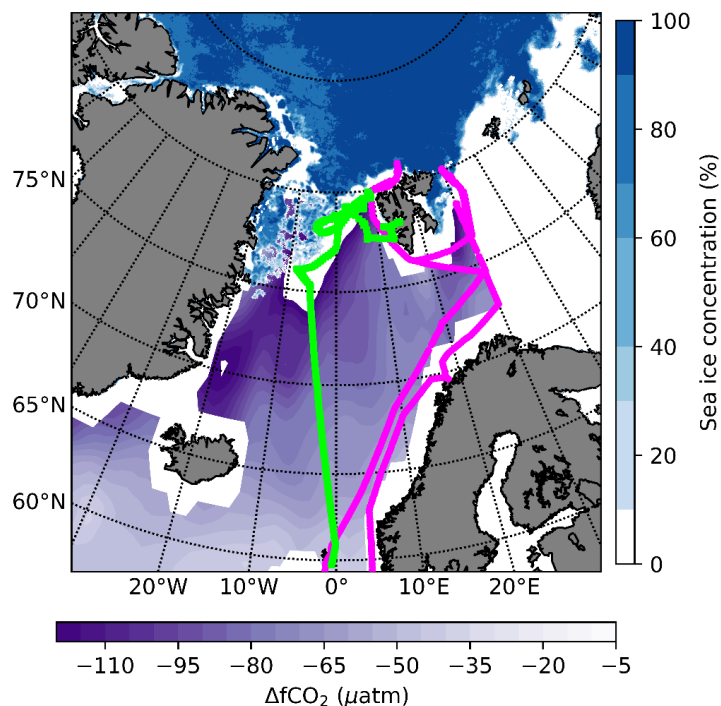
607 The mean uncertainty in hourly EC flux is estimated to be 1.4–3.2 mmol m⁻² day⁻¹, which
608 equates to the relative uncertainty of ~20% in high CO₂ flux regions and ~50% in low CO₂ flux
609 regions. Lengthening the averaging timescale can improve the signal: noise ratio in EC CO₂
610 flux through the reduction of random uncertainty. Auto-covariance analysis of CO₂ flux is used
611 to quantify the optimal averaging timescale (Fig. 7 and 8, Sect. 4.1). The optimal averaging
612 timescale varies between 1 hour for regions of large CO₂ flux (Arctic in our analysis) and at
613 least 3 hours for regions of low CO₂ flux (tropical/sub-tropical Atlantic in our analysis).

614 The measurement uncertainty in EC CO₂ flux contributes directly to scatter in the derived gas
615 transfer velocity, K_{660} . Flux uncertainties determined in this paper are applied to a synthetic
616 K_{660} dataset. This enables a partitioning of the variance in measured K_{660} that is due to EC CO₂
617 flux uncertainty, wind speed, and other processes (10%, 76%, 14% for Arctic cruise JR18007).
618 At a given averaging timescale, a $|\Delta f\text{CO}_2|$ threshold helps to reduce the scatter in K_{660} . A
619 minimum $|\Delta f\text{CO}_2|$ filter of 20 μatm is needed for interpreting hourly K_{660} data, with the signal:
620 noise ratio in K_{660} improving further at higher $|\Delta f\text{CO}_2|$.

621

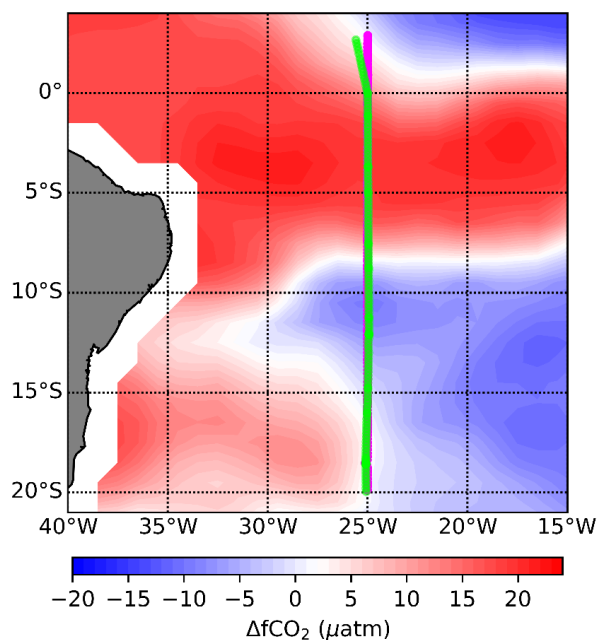
622

623 **Appendix A: Cruise tracks**



624

625 **Figure A1.** Cruise tracks of JR18006 (magenta) and JR18007 (green). The bottom colour bar indicates
626 the CO₂ fugacity difference ($\Delta f\text{CO}_2$) of August 2019 (Bakker et al., 2016; Landschützer et al., 2020),
627 while the right colour bar shows the Arctic sea ice concentrations of 1st August 2019 measured by
628 Advanced Microwave Scanning Radiometer - Earth Observing System Sensor (AMSR-E, Spreen et al.,
629 2008).



630

631 **Figure A2.** Cruise tracks of AMT28 (magenta) and AMT29 (green). The ocean is coloured with the
632 $\Delta f\text{CO}_2$ for October 2018 (Bakker et al., 2016; Landschützer et al., 2020).

633

634 **Appendix B: Integral time scale and variance spectra of CO₂ and vertical wind velocity**

635 Integral time scale is used in the flux uncertainty calculation (Eq. 5 and 7). The definition of
636 integral time scale τ_x of variable x is:

$$637 \quad \tau_x = \frac{1}{\sigma_x^2} \int_0^{\infty} r_{xx}(t) dt \quad (\text{B1})$$

638 where σ_x^2 is the variance of x and r_{xx} is the auto-covariance function of x . t is the shifting time
639 of auto-covariance (which is different from the lag time between w and CO₂ in the EC flux
640 calculation). We can use Eq. B1 to estimate the integral time scale of w and CO₂ directly.
641 However, integration up to infinity is not practical. Instead we can numerically estimate the
642 time scale by determining the time corresponding to the auto-covariance coefficient function
643 (r_{xx}/σ_x^2) value decaying to 1/e (1/e decaying method) or by integrating the auto-covariance
644 function up to the first zero crossing of the function (zero crossing method) (Rannik et al.,
645 2009).



646 One can also use similarity theory to estimate the integral time scale theoretically (Blomquist
647 et al., 2010):

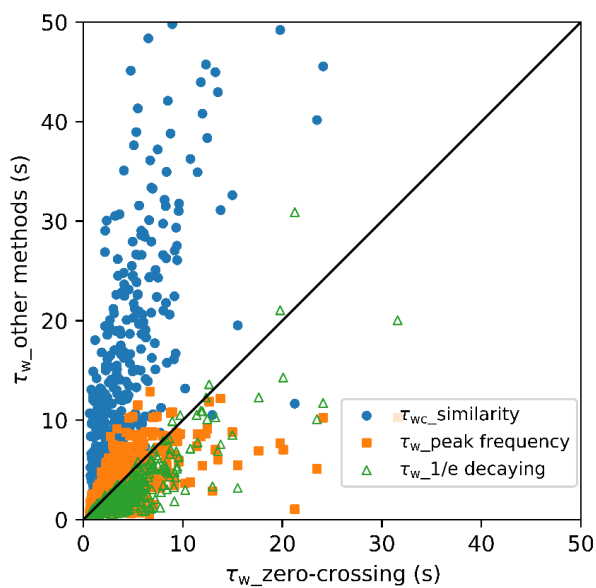
$$648 \quad \tau_w = 2.8 \frac{z}{\bar{u}_r} f_\tau(z/L) \quad (B2)$$

649 Here, \bar{u}_r is the relative wind speed. The similarity function $f_\tau(z/L)$ is described by the stability
650 parameter z/L where z is the observation height (m) and L is the Obukhov length (m)
651 (Blomquist et al., 2010).

652 Yet another method to estimate the integral time scale is from the peak frequency (f_{\max}) in the
653 w variance spectrum (Kaimal and Finnigan, 1994):

$$654 \quad \tau_w = \frac{1}{2\pi f_{\max}} \quad (B3)$$

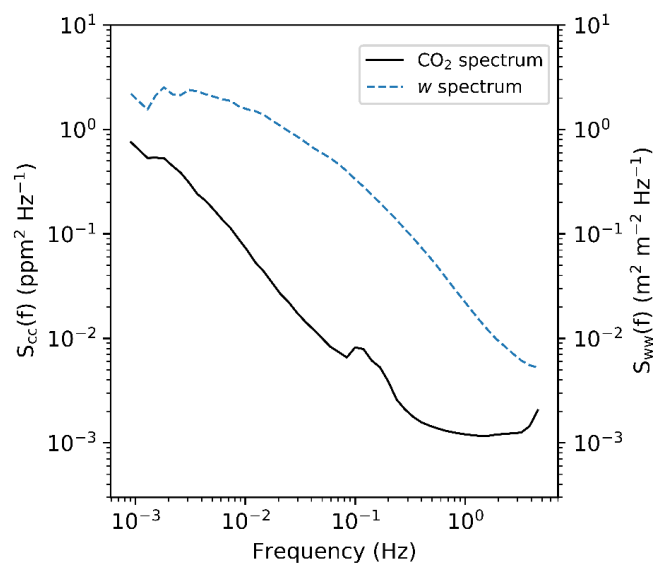
655 The integral time scales of w estimated by these four methods for cruise JR18007 are shown in
656 Figure B1. The integral time scale estimated by the zero crossing method agrees well with the
657 peak frequency estimates using Eq. B3. The 1/e decaying method tends to underestimate the
658 integral time scale, which is generally observed for turbulent signals (Rannik et al., 2009),
659 whereas the similarity method (Eq. B2) considerably overestimates the integral time scale. In
660 this study we use the integral time scale of w from the zero crossing method to estimate the
661 theoretical flux uncertainty (Eq. 5 and 7). The theoretical systematic error estimates (Eq. 8)
662 also require the integral time scale of CO_2 . The integral time scale of CO_2 is difficult to evaluate
663 from the above four methods due to instrument noise. Instead, we estimate it by directly
664 integrating the auto-covariance function (Eq. B1) to a shift time of 200 s (we found no
665 significant difference of the integral time scale when integrating the CO_2 auto-covariance
666 function for shift times ranging from 150 s to 250 s).



667

668 **Figure B1.** Comparison of integral time scales of w estimated by four different methods. Estimated
669 integral time scales from the zero crossing method (integrating the auto-covariance function up to first
670 zero crossing the function) agree well with the estimation of peak frequency method (Eq. B2). However,
671 the similarity method (Eq. B1) overestimates the integral time scale whereas the 1/e decaying method
672 (determining the time needed for the auto-covariance coefficient function value to decay to 1/e) tends
673 to underestimate the integral time scale.

674



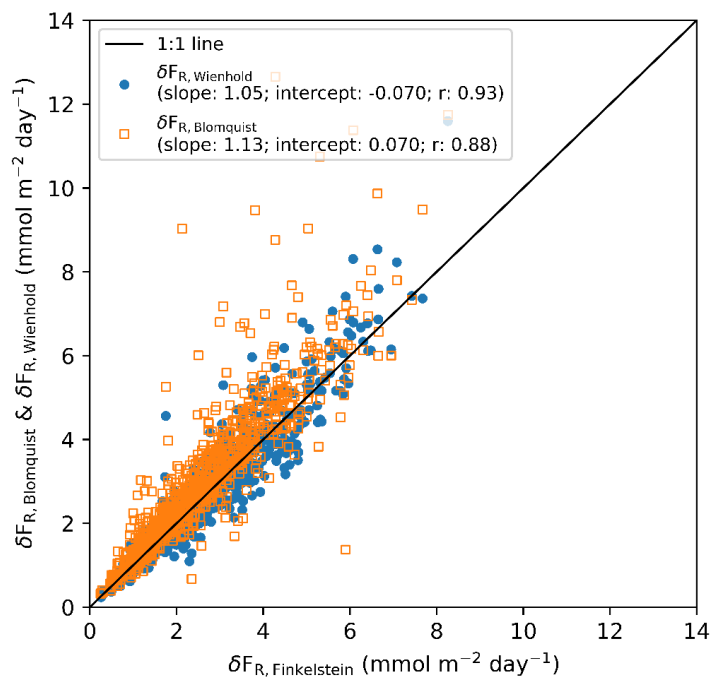
675

676 **Figure B2.** Mean variance spectra for CO₂ and *w* for one Arctic cruise JR18007. The near constant CO₂
677 variance at high frequency (1-5 Hz) indicates the band-limited noise in the CO₂ signal. In contrast, the
678 *w* spectrum does not show a similar band-limited noise at < 10 Hz.

679

680 **Appendix C: Comparison of the uncertainty estimates by different methods**

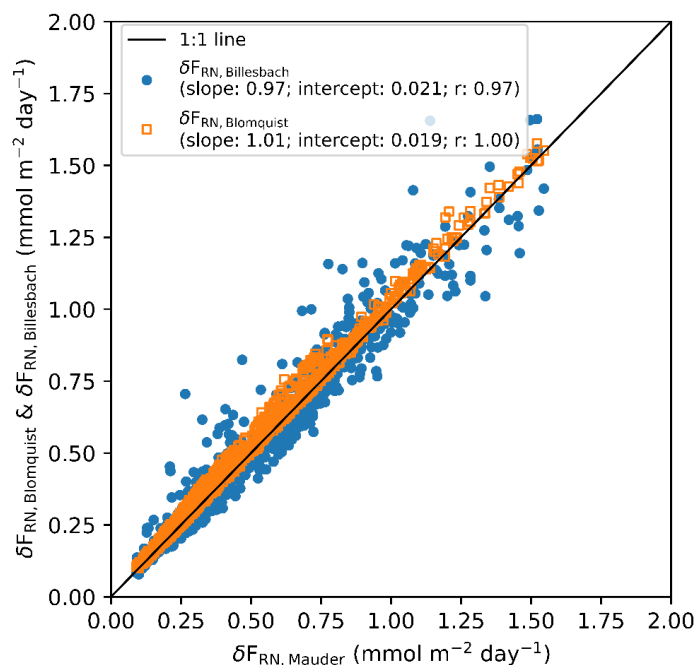
681



682

683 **Figure C1.** Comparison of total random uncertainties in hourly flux estimated by three different
684 methods for the Arctic cruises. The empirical estimates $F_{R, \text{Wienhold}}$ agree well with one of the
685 theoretical estimates $\Delta F_{R, \text{Finkelstein}}$ ($r = 0.93$). The other theoretical estimate $\Delta F_{R, \text{Blomquist}}$ is slightly
686 higher than the random uncertainties $\Delta F_{R, \text{Finkelstein}}$ (slope = 1.13) if the constant in Eq. 8 is set equal
687 to $\sqrt{2}$.

688



689

690 **Figure C2.** Comparison of random error in hourly flux due to instrument white noise, estimated by
691 three different methods for the Arctic cruises. The three uncertainty estimations agree well. The
692 correlation coefficient (r) between $\delta F_{RN, Mauder}$ and $\delta F_{RN, Blomquist}$ is 1 if the constant in Eq. 7 (a) is set
693 to $\sqrt{2}$.

694

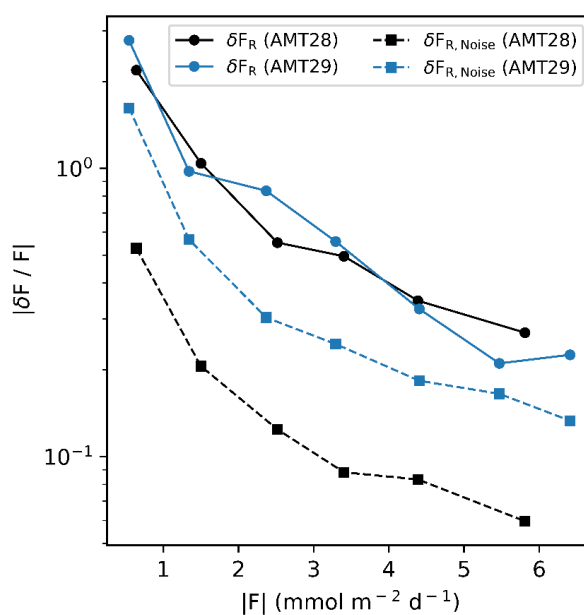
695 **Appendix D: Performance of two gas analysers**

696 Figure D1 shows a comparison between the performance of the Picarro 2311-f and the LI-7200
697 gas analysers. We estimated that the noise of the LI-7200 is on average 3 times higher than that
698 of the Picarro 2311-f (Table 3). Indeed, random error in the CO_2 flux due to the white noise is
699 much higher for the LI-7200 than for the Picarro 2311-f, but the total flux uncertainty of the
700 EC system with the LI-7200 on AMT29 is only slightly higher than that of the EC system with
701 the Picarro 2311-f on AMT28 (Table 4). Again, this is because for both EC systems, sampling
702 error dominates the total random uncertainty, while the contribution of instrument noise (<
703 30%) to the total uncertainty is relatively small (Billesbach, 2011; Langford et al., 2015;
704 Mauder et al., 2013; Rannik et al., 2016). Another often used CRDS gas analyser in EC
705 measurements is the Los Gatos Research (LGR) Fast Greenhouse Gas Analyser (FGGA)



706 (Prytherch et al., 2017). Yang et al. (2016) showed that LGR FGGA is ca. 10 times noisier than
707 the Picarro G2311-f, and as a result the total CO₂ flux uncertainty measured by the LGR is 4
708 times higher than that by the Picarro. From the perspective of measurement noise, Picarro and
709 LI-7200 gas analysers are better suited for air-sea CO₂ flux measurements than the LGR FGGA.

710



711

712 **Figure D1.** Comparison of the relative total random uncertainty and the relative random error
713 component due to white noise for different gas analysers. A Picarro G2311-f gas analyser was used on
714 AMT28 and a LI-7200 infrared gas analyser on AMT29.

715

716

717 *Data availability.* The processed hourly EC CO₂ fluxes and uncertainties can be found in the
718 Supplement of this paper. Raw, high frequency (10 Hz) data are large (tens of gigabytes) and are
719 archived at PML. Please contact the authors directly if you are interested in the raw data.

720

721 *Supplement.* The supplement related to this article is available online at:

722



723 *Author contributions.* TB and MY designed and installed the eddy covariance systems on ships and
724 managed the collections of measurements. VK collected and processed the CO₂ fugacity data. YD
725 processed and analysed the data with the help of MY and TB. YD wrote the paper with input from DB,
726 TB and MY. All authors contributed to and approved the final manuscript.

727

728 *Competing interests.* The authors declare that they have no conflict of interest.

729

730 *Acknowledgements.* We thank captains and crew of the RRS James Clark Ross and RRS Discovery and
731 all those who have helped keep the CO₂ flux systems running. We are extremely grateful to B. J.
732 Butterworth (University of Calgary) for his advice on how to setup and run the automated CO₂ flux
733 system on JCR and how to code the CR6 data logger, as well as to T. J. Smyth (PML) for setting up the
734 remote monitoring of flux data. We also greatly appreciate I. Brown (PML) and D. Phillips for *f*CO₂
735 measurements and P. S. Liss (UEA) for support and helpful comments.

736

737 *Financial support.* This work is funded by the China Scholarship Council (CSC/201906330072). Air-
738 sea CO₂ flux measurements were facilitated by European Space Agency (ESA AMT4oceanSatFlux
739 project, grant no. 4000125730/18/NL/FF/gp) and support from the Natural Environment Research
740 Council (NERC) via PML's contribution to the ORCHESTRA program (NE/N018095/1). The Arctic
741 cruises were also supported by NERC, through the DIAPOD (NE/P006280/2) and ChaOS
742 (NE/P006493/1) projects.

743

744

745

746 **References**

747 Bakker, D. C. E., Pfeil, B., Landa, C. S., Metzl, N., O'Brien, K. M., Olsen, A., Smith, K., Cosca, C., Harasawa,
748 S., Jones, S. D., Nakaoka, S. I., Nojiri, Y., Schuster, U., Steinhoff, T., Sweeney, C., Takahashi, T., Tilbrook, B.,
749 Wada, C., Wanninkhof, R., Alin, S. R., Balestrini, C. F., Barbero, L., Bates, N. R., Bianchi, A. A., Bonou, F.,
750 Boutin, J., Bozec, Y., Burger, E. F., Cai, W. J., Castle, R. D., Chen, L., Chierici, M., Currie, K., Evans, W.,
751 Featherstone, C., Feely, R. A., Fransson, A., Goyet, C., Greenwood, N., Gregor, L., Hankin, S., Hardman-
752 Mountford, N. J., Harlay, J., Hauck, J., Hoppema, M., Humphreys, M. P., Hunt, C. W., Huss, B., Ibáñez, J. S.
753 P., Johannessen, T., Keeling, R., Kitidis, V., Körtzinger, A., Kozyr, A., Krasakopoulou, E., Kuwata, A.,
754 Landschützer, P., Lauvset, S. K., Lefèvre, N., Lo Monaco, C., Manke, A., Mathis, J. T., Merlivat, L., Millero, F.
755 J., Monteiro, P. M. S., Munro, D. R., Murata, A., Newberger, T., Omar, A. M., Ono, T., Paterson, K., Pearce,



- 756 D., Pierrot, D., Robbins, L. L., Saito, S., Salisbury, J., Schlitzer, R., Schneider, B., Schweitzer, R., Sieger, R.,
757 Skjelvan, I., Sullivan, K. F., Sutherland, S. C., Sutton, A. J., Tadokoro, K., Telszewski, M., Tuma, M., Van
758 Heuven, S. M. A. C., Vandemark, D., Ward, B., Watson, A. J. and Xu, S.: A multi-decade record of high-quality
759 fCO₂ data in version 3 of the Surface Ocean CO₂ Atlas (SOCAT), *Earth Syst. Sci. Data*, 8(2), 383–413,
760 doi:10.5194/essd-8-383-2016, 2016.
- 761 Baldocchi, D., Falge, E., Gu, L., Olson, R., Hollinger, D., Running, S., Anthoni, P., Bernhofer, C., Davis, K. and
762 Evans, R.: FLUXNET: A new tool to study the temporal and spatial variability of ecosystem-scale carbon
763 dioxide, water vapor, and energy flux densities, *Bull. Am. Meteorol. Soc.*, 82(11), 2415–2434, 2001.
- 764 Bariteau, L., Helmig, D., Fairall, C. W., Hare, J. E., Hueber, J. and Lang, E. K.: Determination of oceanic ozone
765 deposition by ship-borne eddy covariance flux measurements, *Atmos. Meas. Tech.*, 3(2), 441–455,
766 doi:10.5194/amt-3-441-2010, 2010.
- 767 Bell, T. G., De Bruyn, W., Marandino, C. A., Miller, S. D., Law, C. S., Smith, M. J. and Saltzman, E. S.:
768 Dimethylsulfide gas transfer coefficients from algal blooms in the Southern Ocean, *Atmos. Chem. Phys.*, 15(4),
769 1783–1794, 2015.
- 770 Billesbach, D. P.: Estimating uncertainties in individual eddy covariance flux measurements: A comparison of
771 methods and a proposed new method, *Agric. For. Meteorol.*, 151(3), 394–405,
772 doi:10.1016/j.agrformet.2010.12.001, 2011.
- 773 Blomquist, B. W., Huebert, B. J., Fairall, C. W. and Faloona, I. C.: Determining the sea-air flux of
774 dimethylsulfide by eddy correlation using mass spectrometry, *Atmos. Meas. Tech.*, 3(1), 1–20, doi:10.5194/amt-
775 3-1-2010, 2010.
- 776 Blomquist, B. W., Fairall, C. W., Huebert, B. J. and Wilson, S. T.: Direct measurement of the oceanic carbon
777 monoxide flux by eddy correlation, *Atmos. Meas. Tech.*, 5(12), 3069–3075, doi:10.5194/amt-5-3069-2012,
778 2012.
- 779 Blomquist, B. W., Huebert, B. J., Fairall, C. W., Bariteau, L., Edson, J. B., Hare, J. E. and McGillis, W. R.:
780 Advances in Air-Sea CO₂ Flux Measurement by Eddy Correlation, *Boundary-Layer Meteorol.*, 152(3), 245–
781 276, doi:10.1007/s10546-014-9926-2, 2014.
- 782 Blomquist, B. W., Brumer, S. E., Fairall, C. W., Huebert, B. J., Zappa, C. J., Brooks, I. M., Yang, M., Bariteau,
783 L., Prytherch, J., Hare, J. E., Czerski, H., Matei, A. and Pascal, R. W.: Wind Speed and Sea State Dependencies
784 of Air-Sea Gas Transfer: Results From the High Wind Speed Gas Exchange Study (HiWinGS), *J. Geophys. Res.*
785 *Ocean.*, 122(10), 8034–8062, doi:10.1002/2017JC013181, 2017.
- 786 Broecker, W. S. and Peng, T. H.: Greenhouse Puzzles Part 1 Keeling's World: is CO₂ Greening the Earth, k1-
787 k112, Columbia University, 1993.
- 788 Broecker, W. S., Ledwell, J. R., Takahashi, T., Weiss, R., Merlivat, L., Memery, L., Peng, T., Jahne, B. and
789 Munnich, K. O.: Isotopic versus micrometeorologic ocean CO₂ fluxes: A serious conflict, *J. Geophys. Res.*
790 *Ocean.*, 91(C9), 10517–10527, 1986.



- 791 Businger, J.: Evaluation of the accuracy with which dry deposition can be measured with current
792 micrometeorological techniques, *J. Clim. Appl. Meteorol.*, 25(8), 1100–1124, 1986.
- 793 Butterworth, B. J. and Miller, S. D.: Air-sea exchange of carbon dioxide in the Southern Ocean and Antarctic
794 marginal ice zone, *Geophys. Res. Lett.*, 43(13), 7223–7230, doi:10.1002/2016GL069581, 2016.
- 795 Edson, J. B., Hinton, A. A., Prada, K. E., Hare, J. E. and Fairall, C. W.: Direct covariance flux estimates from
796 mobile platforms at sea, *J. Atmos. Ocean. Technol.*, 15(2), 547–562, doi:10.1175/1520-
797 0426(1998)015<0547:DCFEFM>2.0.CO;2, 1998.
- 798 Edson, J. B., Fairall, C. W., Bariteau, L., Zappa, C. J., Cifuentes-Lorenzen, A., McGillis, W. R., Pezoa, S., Hare,
799 J. E. and Helmig, D.: Direct covariance measurement of CO₂ gas transfer velocity during the 2008 Southern
800 Ocean Gas Exchange Experiment: Wind speed dependency, *J. Geophys. Res. Ocean.*, 116(11),
801 doi:10.1029/2011JC007022, 2011.
- 802 Edson, J. B., Jampana, V., Weller, R. A., Bigorre, S. P., Plueddemann, A. J., Fairall, C. W., Miller, S. D., Mahrt,
803 L., Vickers, D. and Hersbach, H.: On the exchange of momentum over the open ocean, *J. Phys. Oceanogr.*,
804 43(8), 1589–1610, 2013.
- 805 Else, B. G. T., Papakyriakou, T. N., Galley, R. J., Drennan, W. M., Miller, L. A. and Thomas, H.: Wintertime
806 CO₂ fluxes in an Arctic polynya using eddy covariance: Evidence for enhanced air-sea gas transfer during ice
807 formation, *J. Geophys. Res. Ocean.*, 116(9), doi:10.1029/2010JC006760, 2011.
- 808 Fairall, C. W., Hare, J. E., Edson, J. B. and McGillis, W.: Parameterization and micrometeorological
809 measurement of air-sea gas transfer, *Boundary-Layer Meteorol.*, 96(1–2), 63–105,
810 doi:10.1023/a:1002662826020, 2000.
- 811 Finkelstein, P. L. and Sims, P. F.: Sampling error in eddy correlation flux measurements, *J. Geophys. Res.*
812 *Atmos.*, 106(D4), 3503–3509, 2001.
- 813 Flügge, M., Paskyabi, M. B., Reuder, J., Edson, J. B. and Plueddemann, A. J.: Comparison of direct covariance
814 flux measurements from an offshore tower and a buoy, *J. Atmos. Ocean. Technol.*, 33(5), 873–890,
815 doi:10.1175/JTECH-D-15-0109.1, 2016.
- 816 Friedlingstein, P., O’Sullivan, M., Jones, M. W., Andrew, R. M., Hauck, J., Olsen, A., Peters, G. P., Peters, W.,
817 Pongratz, J., Sitch, S., Le Quéré, C., Canadell, J. G., Ciais, P., Jackson, R. B., Alin, S., Aragão, L. E. O. C.,
818 Arneeth, A., Arora, V., Bates, N. R., Becker, M., Benoit-Cattin, A., Bittig, H. C., Bopp, L., Bultan, S., Chandra,
819 N., Chevallier, F., Chini, L. P., Evans, W., Florentie, L., Forster, P. M., Gasser, T., Gehlen, M., Gilfillan, D.,
820 Gkritzalis, T., Gregor, L., Gruber, N., Harris, I., Hartung, K., Haverd, V., Houghton, R. A., Ilyina, T., Jain, A.
821 K., Joetzier, E., Kadono, K., Kato, E., Kitidis, V., Korsbakken, J. I., Landschützer, P., Lefèvre, N., Lenton, A.,
822 Lienert, S., Liu, Z., Lombardozi, D., Marland, G., Metzl, N., Munro, D. R., Nabel, J. E. M. S., Nakaoka, S.-I.,
823 Niwa, Y., O’Brien, K., Ono, T., Palmer, P. I., Pierrot, D., Poulter, B., Resplandy, L., Robertson, E., Rödenbeck,
824 C., Schwinger, J., Séférian, R., Skjelvan, I., Smith, A. J. P., Sutton, A. J., Tanhua, T., Tans, P. P., Tian, H.,
825 Tilbrook, B., van der Werf, G., Vuichard, N., Walker, A. P., Wanninkhof, R., Watson, A. J., Willis, D.,
826 Wiltshire, A. J., Yuan, W., Yue, X. and Zaehle, S.: Global Carbon Budget 2020, *Earth Syst. Sci. Data*, 12(4),



- 827 3269–3340, doi:10.5194/essd-12-3269-2020, 2020.
- 828 Garbe, C. S., Rutgersson, A., Boutin, J., De Leeuw, G., Delille, B., Fairall, C. W., Gruber, N., Hare, J., Ho, D.
829 T. and Johnson, M. T.: Transfer across the air-sea interface, in *Ocean-atmosphere interactions of gases and*
830 *particles*, pp. 55–112, Springer, Berlin, Heidelberg., 2014.
- 831 Ho, D. T., Law, C. S., Smith, M. J., Schlosser, P., Harvey, M. and Hill, P.: Measurements of air-sea gas
832 exchange at high wind speeds in the Southern Ocean: Implications for global parameterizations, *Geophys. Res.*
833 *Lett.*, 33(16), 2006.
- 834 Ikawa, H., Faloona, I., Kochendorfer, J., Paw U, K. T. and Oechel, W. C.: Air-sea exchange of CO₂ at a
835 Northern California coastal site along the California Current upwelling system, *Biogeosciences*, 10(7), 4419–
836 4432, doi:10.5194/bg-10-4419-2013, 2013.
- 837 JCGM, J.: Evaluation of measurement data—Guide to the expression of uncertainty in measurement, *Int. Organ.*
838 *Stand. Geneva ISBN, 50, 134, 2008.*
- 839 Jones, E. P. and Smith, S. D.: A first measurement of sea-air CO₂ flux by eddy correlation, *J. Geophys. Res.*,
840 82(37), 5990–5992, 1977.
- 841 Kaimal, J. C. and Finnigan, J. J.: *Atmospheric boundary layer flows: their structure and measurement*, Oxford
842 university press., 1994.
- 843 Kaimal, J. C., Wyngaard, J. C., Izumi, Y. and Cote, O. R.: Spectral characteristics of surface-layer turbulence,
844 *Q. J. R. Meteorol. Soc.*, 098(417), 563–589, doi:10.1256/smsqj.41706, 1972.
- 845 Kohsiek, W.: Water vapor cross-sensitivity of open path H₂O/CO₂ sensors, *J. Atmos. Ocean. Technol.*, 17(3),
846 299–311, doi:10.1175/1520-0426(2000)017<0299:WVCSOO>2.0.CO;2, 2000.
- 847 Kondo, F. and Tsukamoto, O.: Air-sea CO₂ flux by eddy covariance technique in the equatorial Indian Ocean, *J.*
848 *Oceanogr.*, 63(3), 449–456, doi:10.1007/s10872-007-0040-7, 2007.
- 849 Landschützer, P., Gruber, N. and Bakker, D. C. E.: An observation-based global monthly gridded sea surface
850 pCO₂ product from 1982 onward and its monthly climatology (NCEI Accession 0160558), Version 5.5, NOAA
851 National Centers for Environmental Information, Dataset, <https://doi.org/10.7289/V5Z899N6>, 2020.
- 852 Landwehr, S., Miller, S. D., Smith, M. J., Saltzman, E. S. and Ward, B.: Analysis of the PKT correction for
853 direct CO₂ flux measurements over the ocean, *Atmos. Chem. Phys.*, 14(7), 3361–3372, doi:10.5194/acp-14-
854 3361-2014, 2014.
- 855 Landwehr, S., Miller, S. D., Smith, M. J., Bell, T. G., Saltzman, E. S. and Ward, B.: Using eddy covariance to
856 measure the dependence of air-sea CO₂ exchange rate on friction velocity, *Atmos. Chem. Phys.*, 18(6), 4297–
857 4315, doi:10.5194/acp-18-4297-2018, 2018.
- 858 Langford, B., Acton, W., Ammann, C., Valach, A. and Nemitz, E.: Eddy-covariance data with low signal-to-
859 noise ratio: Time-lag determination, uncertainties and limit of detection, *Atmos. Meas. Tech.*, 8(10), 4197–4213,
860 doi:10.5194/amt-8-4197-2015, 2015.



- 861 Lauvset, S. K., McGillis, W. R., Bariteau, L., Fairall, C. W., Johannessen, T., Olsen, A. and Zappa, C. J.: Direct
862 measurements of CO₂ flux in the Greenland Sea, *Geophys. Res. Lett.*, 38(12), 2011.
- 863 Lenschow, D. H. and Kristensen, L.: Uncorrelated noise in turbulence measurements, *J. Atmos. Ocean.*
864 *Technol.*, 2(1), 68–81, 1985.
- 865 Lenschow, D. H., Mann, J. and Kristensen, L.: How long is long enough when measuring fluxes and other
866 turbulence statistics? NCAR Tech. Note, NCAR/TN-389, 53 Natl. Cent. for Atmos. Res., Boulder, Colo., 1993.
- 867 Lenschow, D. H., Mann, J. and Kristensen, L.: How long is long enough when measuring fluxes and other
868 turbulence statistics? *J. Atmos. Ocean. Technol.*, 11(3), 661–673, doi:10.1175/1520-
869 0426(1994)011<0661:HLILEW>2.0.CO;2, 1994.
- 870 Lenschow, D. H., Wulfmeyer, V. and Senff, C.: Measuring second- through fourth-order moments in noisy data,
871 *J. Atmos. Ocean. Technol.*, 17(10), 1330–1347, doi:10.1175/1520-0426(2000)017<1330:MSTFOM>2.0.CO;2,
872 2000.
- 873 Loescher, H. W., Law, B. E., Mahrt, L., Hollinger, D. Y., Campbell, J. and Wofsy, S. C.: Uncertainties in, and
874 interpretation of, carbon flux estimates using the eddy covariance technique, *J. Geophys. Res. Atmos.*, 111(21),
875 1–19, doi:10.1029/2005JD006932, 2006.
- 876 Mahrt, L.: Flux sampling errors for aircraft and towers, *J. Atmos. Ocean. Technol.*, 15(2), 416–429,
877 doi:10.1175/1520-0426(1998)015<0416:FSEFAA>2.0.CO;2, 1998.
- 878 Mauder, M., Cuntz, M., Driie, C., Graf, A., Rebmann, C., Schmid, H. P., Schmidt, M. and Steinbrecher, R.: A
879 strategy for quality and uncertainty assessment of long-term eddy-covariance measurements, *Agric. For.*
880 *Meteorol.*, 169, 122–135, doi:10.1016/j.agrformet.2012.09.006, 2013.
- 881 McGillis, W. R., Edson, J. B., Ware, J. D., Dacey, J. W. H., Hare, J. E., Fairall, C. W. and Wanninkhof, R.:
882 Carbon dioxide flux techniques performed during GasEx-98, *Mar. Chem.*, 75(4), 267–280, doi:10.1016/S0304-
883 4203(01)00042-1, 2001.
- 884 McGillis, W. R., Edson, J. B., Zappa, C. J., Ware, J. D., McKenna, S. P., Terray, E. A., Hare, J. E., Fairall, C.
885 W., Drennan, W. and Donelan, M.: Air-sea CO₂ exchange in the equatorial Pacific, *J. Geophys. Res. Ocean.*,
886 109(C8), 2004.
- 887 Miller, S. D., Marandino, C. and Saltzman, E. S.: Ship-based measurement of air-sea CO₂ exchange by eddy
888 covariance, *J. Geophys. Res. Atmos.*, 115(D2), 1–14, doi:10.1029/2009JD012193, 2010.
- 889 Moat, B. and Yelland, M.: Airflow distortion at instrument sites on the RRS James Clark Ross during the
890 WAGES project, No. 12, National Oceanography Centre Internal Document, National Oceanography Centre,
891 Southampton, 2015.
- 892 Moat, B. I., Yelland, M. J. and Cooper, E. B.: The airflow distortion at instruments sites on the RRS" James
893 Cook", National Oceanography Centre Southampton Research and Consultancy Report 11, National
894 Oceanography Centre, Southampton, 44pp, 2006.



- 895 Nightingale, P. D., Malin, G., Law, C. S., Watson, A. J., Liss, P. S., Liddicoat, M. I., Boutin, J. and Upstill-
896 Goddard, R. C.: In situ evaluation of air-sea gas exchange parameterizations using novel conservative and
897 volatile tracers, *Global Biogeochem. Cycles*, 14(1), 373–387, doi:10.1029/1999GB900091, 2000.
- 898 Nilsson, E., Bergström, H., Rutgersson, A., Podgrajsek, E., Wallin, M. B., Bergström, G., Dellwik, E.,
899 Landwehr, S. and Ward, B.: Evaluating humidity and sea salt disturbances on CO₂ flux measurements, *J. Atmos.*
900 *Ocean. Technol.*, 35(4), 859–875, doi:10.1175/JTECH-D-17-0072.1, 2018.
- 901 Post, H., Hendricks Franssen, H. J., Graf, A., Schmidt, M. and Vereecken, H.: Uncertainty analysis of eddy
902 covariance CO₂ flux measurements for different EC tower distances using an extended two-tower approach,
903 *Biogeosciences*, 12(4), 1205–1221, doi:10.5194/bg-12-1205-2015, 2015.
- 904 Prytherch, J., Yelland, M. J., Pascal, R. W., Moat, B. I., Skjelvan, I. and Neill, C. C.: Direct measurements of
905 the CO₂ flux over the ocean: Development of a novel method, *Geophys. Res. Lett.*, 37(3),
906 doi:10.1029/2009GL041482, 2010.
- 907 Prytherch, J., Brooks, I. M., Crill, P. M., Thornton, B. F., Salisbury, D. J., Tjernström, M., Anderson, L. G.,
908 Geibel, M. C. and Humborg, C.: Direct determination of the air-sea CO₂ gas transfer velocity in Arctic sea ice
909 regions, *Geophys. Res. Lett.*, 44(8), 3770–3778, 2017.
- 910 Rannik, Ü., Mammarella, I., Aalto, P., Keronen, P., Vesala, T. and Kulmala, M.: Long-term aerosol particle flux
911 observations part I: Uncertainties and time-average statistics, *Atmos. Environ.*, 43(21), 3431–3439,
912 doi:10.1016/j.atmosenv.2009.02.049, 2009.
- 913 Rannik, Ü., Peltola, O. and Mammarella, I.: Random uncertainties of flux measurements by the eddy covariance
914 technique, *Atmos. Meas. Tech.*, 9(10), 5163–5181, doi:10.5194/amt-9-5163-2016, 2016.
- 915 Smith, S. D. and Jones, E. P.: Evidence for wind-pumping of air-sea gas exchange based on direct
916 measurements of CO₂ fluxes, *J. Geophys. Res. Ocean.*, 90(C1), 869–875, 1985.
- 917 Spreen, G., Kaleschke, L. and Heygster, G.: Sea ice remote sensing using AMSR-E 89-GHz channels, *J.*
918 *Geophys. Res. Ocean.*, 113(C2), doi:10.1029/2005JC003384, 2008.
- 919 Takahashi, T., Sutherland, S. C., Wanninkhof, R., Sweeney, C., Feely, R. A., Chipman, D. W., Hales, B.,
920 Friederich, G., Chavez, F., Sabine, C., Watson, A., Bakker, D. C. E., Schuster, U., Yoshikawa-Inoue, H., Ishii,
921 M., Midorikawa, T., Nojiri, Y., Körtzinger, A., Steinhoff, T., Hoppema, M., Olafsson, J., Arnarson, T. S.,
922 Johannessen, T., Olsen, A., Bellerby, R., Wong, C. S., Delille, B., Bates, N. R. and de Baar, H. J. W.:
923 Climatological mean and decadal change in surface ocean pCO₂, and net sea–air CO₂ flux over the global
924 oceans, *Deep Sea Res. Part II Top. Stud. Oceanogr.*, 56(8–10), 554–577, doi:10.1016/J.DSR2.2008.12.009,
925 2009.
- 926 Tsukamoto, O., Kondo, F. and Kamei, Y.: Overestimation of downward air-sea eddy CO₂ flux due to optical
927 window contamination of open-path gas analyzer, *SOLA*, 10, 117–121, 2014.
- 928 Wanninkhof, R.: Relationship between wind speed and gas exchange over the ocean revisited, *Limnol.*
929 *Oceanogr. Methods*, 12(6), 351–362, doi:10.4319/lom.2014.12.351, 2014.



- 930 Weiss, A., Kuss, J., Peters, G. and Schneider, B.: Evaluating transfer velocity-wind speed relationship using a
931 long-term series of direct eddy correlation CO₂ flux measurements, *J. Mar. Syst.*, 66(1–4), 130–139,
932 doi:10.1016/j.jmarsys.2006.04.011, 2007.
- 933 Wesely, M. L., Cook, D. R., Hart, R. L. and Williams, R. M.: Air-sea exchange of CO₂ and evidence for
934 enhanced upward fluxes, *J. Geophys. Res. Ocean.*, 87(C11), 8827–8832, 1982.
- 935 Wienhold, F. G., Welling, M. and Harris, G. W.: Micrometeorological measurement and source region analysis
936 of nitrous oxide fluxes from an agricultural soil, *Atmos. Environ.*, 29(17), 2219–2227, 1995.
- 937 Woolf, D. K., Shutler, J. D., Goddijn-Murphy, L., Watson, A. J., Chapron, B., Nightingale, P. D., Donlon, C. J.,
938 Piskozub, J., Yelland, M. J., Ashton, I., Holding, T., Schuster, U., Girard-Ardhuin, F., Grouazel, A., Piolle, J. F.,
939 Warren, M., Wrobel-Niedzwiecka, I., Land, P. E., Torres, R., Prytherch, J., Moat, B., Hanafin, J., Ardhuin, F.
940 and Paul, F.: Key uncertainties in the recent air-sea flux of CO₂, *Global Biogeochem. Cycles*, 33(12), 1548–
941 1563, doi:10.1029/2018GB006041, 2019.
- 942 Wyngaard, J. C.: *Turbulence in the Atmosphere Part 1, Chapt 2, Getting to know turbulence*, p27-54
943 Cambridge University Press., 2010.
- 944 Yang, M., Nightingale, P. D., Beale, R., Liss, P. S., Blomquist, B. and Fairall, C.: Atmospheric deposition of
945 methanol over the Atlantic Ocean, *Proc. Natl. Acad. Sci. U. S. A.*, 110(50), 20034–20039,
946 doi:10.1073/pnas.1317840110, 2013.
- 947 Yang, M., Prytherch, J., Kozlova, E., Yelland, M. J., Parenkat Mony, D. and Bell, T. G.: Comparison of two
948 closed-path cavity-based spectrometers for measuring air-water CO₂ and CH₄ fluxes by eddy covariance,
949 *Atmos. Meas. Tech.*, 9(11), 5509–5522, doi:10.5194/amt-9-5509-2016, 2016.
- 950 Yelland, M. J., Moat, B. I., Taylor, P. K., Pascal, R. W., Hutchings, J. and Cornell, V. C.: Wind stress
951 measurements from the open ocean corrected for airflow distortion by the ship, *J. Phys. Oceanogr.*, 28(7), 1511–
952 1526, doi:10.1175/1520-0485(1998)028<1511:WSMFTO>2.0.CO;2, 1998.
- 953
- 954